

1                   **LegacyClimate 1.0: A dataset of pollen-based climate**  
2                   **reconstructions from 2594 Northern Hemisphere sites covering the**  
3                   **last 30 ka and beyond**

4                   Ulrike Herzschuh<sup>1,2,3</sup>, Thomas Böhmer<sup>1</sup>, Chenzhi Li<sup>1,2</sup>, Manuel Chevalier<sup>4,5</sup>, Raphaël Hébert<sup>1</sup>, Anne  
5                   Dallmeyer<sup>6</sup>, Xianyong Cao<sup>1,7</sup>, Nancy H. Bigelow<sup>8</sup>, Larisa Nazarova<sup>1,9</sup>, Elena Y. Novenko<sup>10,11</sup>, Jungjae  
6                   Park<sup>12,13</sup>, Odile Peyron<sup>14</sup>, Natalia A. Rudaya<sup>15,16</sup>, Frank Schlütz<sup>17,18</sup>, Lyudmila S. Shumilovskikh<sup>18</sup>,  
7                   Pavel E. Tarasov<sup>19</sup>, Yongbo Wang<sup>20</sup>, Ruilin Wen<sup>21,22</sup>, Qinghai Xu<sup>23</sup>, Zhuo Zheng<sup>24,25</sup>

8                   <sup>1</sup> Polar Terrestrial Environmental Systems, Alfred Wegener Institute Helmholtz Centre for Polar and  
9                   Marine Research, Telegrafenberg A45, 14473 Potsdam, Germany

10                  <sup>2</sup> Institute of Environmental Science and Geography, University of Potsdam, Karl-Liebknecht-Str. 24-  
11                  25, 14476 Potsdam, Germany

12                  <sup>3</sup> Institute of Biochemistry and Biology, University of Potsdam, Karl-Liebknecht-Str. 24-25, 14476  
13                  Potsdam, Germany

14                  <sup>4</sup> Institute of Geosciences, Sect. Meteorology, Rheinische Friedrich-Wilhelms-Universität Bonn, Auf  
15                  dem Hügel 20, 53121 Bonn, Germany

16                  <sup>5</sup> Institute of Earth Surface Dynamics IDYST, Faculté des Géosciences et l'Environnement, University  
17                  of Lausanne, Bâtiment Géopolis, 1015 Lausanne, Switzerland

18                  <sup>6</sup> Max Planck Institute for Meteorology, Bundesstrasse 53, 20146 Hamburg, Germany

19                  <sup>7</sup> Alpine Paleoecology and Human Adaptation Group (ALPHA), State Key Laboratory of Tibetan  
20                  Plateau Earth System, and Resources and Environment (TPESRE), Institute of Tibetan Plateau  
21                  Research, Chinese Academy of Sciences, 100101 Beijing, China

22                  <sup>8</sup> Alaska Quaternary Center, University of Alaska Fairbanks, Fairbanks, Alaska 99775, USA

23                  <sup>9</sup> Kazan Federal University, Kremlyovskaya str. 18, 420008 Kazan, Russia

- 24 <sup>10</sup> Lomonosov Moscow State University, Faculty of geography, Leniskie gory 1, 119991 Moscow,  
25 Russia
- 26 <sup>11</sup> Department of Quaternary Paleogeography, Institute of Geography Russian Academy of Science,  
27 Staromonrtny lane, 29, 119017, Moscow, Russia
- 28 <sup>12</sup> Department of Geography, Seoul National University, 1 Gwanak-ro, Gwanak-gu, Seoul, 08826,  
29 Republic of Korea
- 30 <sup>13</sup> Institute for Korean Regional Studies, Seoul National University, 1 Gwanak-ro, Gwanak-gu, Seoul,  
31 08826, Republic of Korea
- 32 <sup>14</sup> Institut des Sciences de l'Evolution de Montpellier, Université de Montpellier, CNRS UMR 5554,  
33 Montpellier, France
- 34 <sup>15</sup> PaleoData Lab, Institute of Archaeology and Ethnography, Siberian Branch, Russian Academy of  
35 Sciences, Pr. Akademika 36 Lavrentieva 17, 630090 Novosibirsk, Russia
- 36 <sup>16</sup> Biological Institute, Tomsk State University, Pr. Lenina, 26, Tomsk, 634050, Russia
- 37 <sup>17</sup> Lower Saxony Institute for Historical Coastal Research, D-26382 Wilhelmshaven, Germany
- 38 <sup>18</sup> Department of Palynology and Climate Dynamics, Albrecht-von-Haller Institute for Plant Sciences,  
39 University of Göttingen, Untere Karspüle 2, 37073 Göttingen, Germany
- 40 <sup>19</sup> Freie Universität Berlin, Institute of Geological Sciences, Palaeontology Section, Malteserstrasse  
41 74-100, Building D, 12249 Berlin, Germany
- 42 <sup>20</sup> College of Resource Environment and Tourism, Capital Normal University, 105 West 3rd Ring Rd N,  
43 100048 Beijing, China
- 44 <sup>21</sup> Key Laboratory of Cenozoic Geology and Environment, Institute of Geology and Geophysics,  
45 Chinese Academy of Sciences, 19 Beitucheng West Road, Chaoyang District, 100029 Beijing, China
- 46 <sup>22</sup> CAS Center for Excellence in Life and Paleoenvironment, 100044 Beijing, China
- 47 <sup>23</sup> School of Geographic Sciences, Hebei Normal University, 050024 Shijiazhuang, China

48 <sup>24</sup> Guangdong Key Lab of Geodynamics and Geohazards, School of Earth Sciences and Engineering,  
49 Sun Yat-sen University, 519082 Zhuhai, China

50 <sup>25</sup> Southern Marine Science and Engineering Guangdong Laboratory (Zhuhai), 519082 Zhuhai, China

51 **Correspondence:** Ulrike Herzschuh (Ulrike.Herzschuh@awi.de)

52

53 **Abstract.** Here we describe the LegacyClimate 1.0, a dataset of the reconstruction of mean July  
54 temperature ( $T_{\text{July}}$ ), mean annual temperature ( $T_{\text{ann}}$ ), and annual precipitation ( $P_{\text{ann}}$ ) from 2594 fossil  
55 pollen records from the Northern Hemisphere spanning the entire Holocene with some records reaching  
56 back to the Last Glacial. Two reconstruction methods, the Modern Analogue Technique (MAT) and  
57 Weighted-Averaging Partial-Least Squares regression (WA-PLS) reveal similar results regarding spatial  
58 and temporal patterns. To reduce the impact of precipitation on temperature reconstruction and vice  
59 versa, we also provide reconstructions using tailored modern pollen data limiting the range of the  
60 corresponding other climate variables. We assess the reliability of the reconstructions using information  
61 from the spatial distributions of the root-mean-squared error of prediction and reconstruction significance  
62 tests. The dataset is beneficial for synthesis studies of proxy-based reconstructions and to evaluate the  
63 output of climate models and thus help to improve the models themselves. We provide our compilation  
64 of reconstructed  $T_{\text{July}}$ ,  $T_{\text{ann}}$ , and  $P_{\text{ann}}$  as open-access datasets at PANGAEA  
65 (<https://doi.pangaea.de/10.1594/PANGAEA.930512>; Herzschuh et al., 2021). R code for the  
66 reconstructions is provided at Zenodo (<https://doi.org/10.5281/zenodo.5910989>; Herzschuh et al.,  
67 2022b), including harmonized open-access modern and fossil datasets used for the reconstructions, so  
68 that customized reconstructions can be easily established.

69

## 70 **1 Introduction**

71 The comparison of climate model outputs with climate data is essential for model improvements (Eyring  
72 et al., 2019). The extratropical Northern Hemisphere is of particular interest because it is known for  
73 complex spatial and temporal temperature and precipitation patterns. However, the period for which  
74 instrumental observations are available is only of limited use to validate simulations, in particular when  
75 assessing climate response to natural climate drivers because it is too short and because it is impacted

76 by human-induced greenhouse gas forcing. Climate proxy data derived from natural archives are  
77 therefore of great value.

78 Previous proxy-based climate inferences have contributed to major debates about Holocene climate  
79 change. For example, while simulations indicate gradual warming of the Holocene, temperature proxy  
80 data syntheses rather support a mid-Holocene optimum which resulted in the “Holocene conundrum”  
81 debate (Liu et al., 2014). While the debate has progressed since new proxy-based syntheses can help  
82 to understand regional differences and contribute further to the debate. Qualitative proxy-based  
83 inferences indicate that the mid-Holocene in the Northern Hemisphere mid-latitudes was rather dry and  
84 warm compared with present-day in agreement with modeling outputs (Routson et al., 2019). Also,  
85 quantitative precipitation reconstructions from Eastern and Central Asia unveiled the complex monsoon-  
86 westerlies interactions (Chen et al., 2019; Herzsuh et al., 2019). However, evaluating modeling  
87 outputs using proxy-based reconstructions is a complex task and strongly depend on the purpose of the  
88 proxy data-model comparison study (e.g. the purpose of an evaluation could either target the mean or  
89 site-specific changes, or it could target relative changes or absolute values, or the purpose could be to  
90 infer spatial or temporal climate variability at specific scales, etc.). All these types of evaluation require  
91 a specific handling of the proxy-data and have to be considered for proxy-model comparisons.

92 Fossil pollen records are well-established in their use as a palaeoecological and palaeoclimatological  
93 proxy and of great value as indicators of past environmental and climatic change for many decades.  
94 Considerable efforts have been made to establish regional, continental and even global data repositories  
95 like the North American Pollen Database (NAPD; <https://www.ncei.noaa.gov/products/paleoclimatology>,  
96 last access: 1 July 2020), the European Pollen Database  
97 (EPD; <http://www.europeanpollendatabase.net/index.php>, last access: 1 July 2020) and the Neotoma  
98 Paleocology Database (<https://www.neotomadb.org/>, last access: 1 April 2021; Williams et al., 2018).  
99 Pollen data from archives across multiple environmental settings such as lakes, wetlands, or marine  
100 sediments, have been widely used to quantitatively reconstruct past vegetation and climate variables  
101 (Birks, 2019; Chevalier et al., 2020). ~~Pollen data are the only land-derived proxy data that have sufficient~~  
102 ~~temporal and spatial coverage to allow for climate model evaluation of the late Quaternary period.~~  
103 Among land-derived proxy data, pollen are particularly suitable for temporarily and spatially high-  
104 resolution evaluation of climate model simulations of the late Quaternary period. A number of methods  
105 have been proposed for making pollen-based climate reconstructions (Chevalier et al., 2020): among  
106 them, classification approaches like the Modern Analogue Technique (MAT) or regression approaches

107 like Weighted-Averaging Partial-Least Squares regression (WA-PLS) are most commonly used. MAT  
108 and WA-PLS rely on extensive collections of modern [spectra training data](#). Hence, designing a robust  
109 calibration dataset from modern pollen assemblages is a crucial part of the reconstruction process. A  
110 suitable calibration dataset should cover a wide range of climatic and environmental gradients in order  
111 to represent an empirical relationship between pollen assemblages and climate (Birks et al., 2010;  
112 Chevalier et al., 2020). Like with fossil pollen records, data syntheses and repositories also exist for  
113 modern surface pollen data e.g. for North America (Whitmore et al., 2005), Eurasia (Davis et al., 2013  
114 and 2020) and China (Cao et al., 2013; Herzschuh et al., 2019).

115 For temperature reconstruction time-series, several broad-scale syntheses exist; however, either they  
116 originate from different proxies (Kaufman et al., 2020a and 2020b) or are restricted to certain continents  
117 or regions or/and are poorly documented (Mauri et al., 2015; Marsicek et al., 2018; Routson et al., 2019).  
118 Temperature reconstructions from extratropical Asia are mostly lacking. Precipitation syntheses are  
119 available from Europe (Mauri et al., 2015), North America (Gajewski, 2000) and China and Mongolia  
120 (Herzschuh et al., 2019) but, hitherto, no global or hemispheric syntheses of quantitative precipitation  
121 changes are available for the Holocene.

122 In a recent effort, we synthesized and taxonomically harmonized pollen records available in the Neotoma  
123 Paleocology Database (Williams et al., 2018) and additional records from China and Siberia (Cao et  
124 al., 2013 and 2020) into a global Late Quaternary fossil pollen dataset (LegacyPollen 1.0; Herzschuh et  
125 al., 2022c) and revised all chronologies of those records using a Bayesian approach that allows for the  
126 inference of temporal uncertainties (LegacyAge 1.0; Li et al., 2022). Here, in the third part of [a series of](#)  
127 interconnected studies, we present the pollen-based reconstruction of mean July temperature ( $T_{July}$ ),  
128 mean annual temperature ( $T_{ann}$ ) and annual precipitation ( $P_{ann}$ ) including reconstruction and temporal  
129 uncertainties as well as quality measures from 2594 records from the Northern Hemisphere using WA-  
130 PLS and MAT (LegacyClimate 1.0; this study).

131

## 132 **2 Methods**

### 133 **2.1 Input data**

134 The objective of this study is to create a dataset of quantitative reconstructions of  $T_{July}$ ,  $T_{ann}$  and  $P_{ann}$   
135 spanning the last 30 ka and beyond from fossil pollen records. These variables (or variables highly

136 correlated to them) were shown to explain most variance in the modern pollen data ( $T_{\text{July}}$ ,  $P_{\text{ann}}$ ) or are  
137 typically used in syntheses ~~is studies and proxy-model comparison studies~~ ( $T_{\text{ann}}$ ). Accordingly, we  
138 selected these three variables. We used the fossil data set compiled in LegacyPollen 1.0 (stored on the  
139 PANGAEA open data repository database and presented in Herzschuh et al., 2022c) that integrates  
140 pollen records archived in the Neotoma Paleoecology Database, a dataset from Eastern and Central  
141 Asia (Cao et al., 2013; Herzschuh et al., 2019) and a dataset from Northern Asia (Cao et al., 2020).  
142 Ages were taken from the “Bacon” (Blaauw and Christen, 2011) age-depth models presented in Li et al.  
143 (2022, LegacyAge 1.0), and for each record, we provide an ensemble of 1000 realizations of the age-  
144 depth model in our data product so that it can be used to account for chronological uncertainty on the  
145 reconstructions. As the chronological and reconstruction errors are independent, they can be added in  
146 quadrature to obtain the combined error. With this information, users can easily produce curves with all  
147 relevant uncertainties as exemplary shown in Appendix Figure 1.

148 We compiled the fossil data into four sub-continental datasets for Eastern North America ( $<104^{\circ}\text{W}$ ;  
149 Williams et al., 2000), Western North America, Europe ( $<43^{\circ}\text{E}$ ) and Asia ( $>43^{\circ}\text{E}$ ). We restricted the  
150 analyses to the 70 most common taxa on each continent to reduce computational power after making  
151 sure that higher taxa number would not substantially improve model statistics in climate reconstructions.  
152 The number of taxa is limited by the modern training dataset from North America, which contains 70  
153 taxa after applying our taxa harmonization routine (see details in Herzschuh et al., 2022c). We therefore  
154 restricted the number of taxa in all fossil datasets to keep the taxa comparable for the reconstructions.  
155 To identify the most common taxa we used Hill’s  $N_2$  diversity index (i.e., the effective number of  
156 occurrences of a species in the dataset; Hill, 1973). For all analyses, square-root percentages were  
157 used if not indicated otherwise.

158 A modern pollen training dataset comprised of 15379 sites includes datasets from Eurasia (EMPD1,  
159 Davis et al. 2013; EMPD2, Davis et al. 2020; Herzschuh et al., 2019; Tarasov et al., 2011) and North  
160 America (Whitmore et al., 2005). The modern pollen datasets were taxonomically harmonized in  
161 accordance with the fossil pollen dataset ~~(see details in Herzschuh et al., 2022c).~~

162 The site-specific  $T_{\text{ann}}$ ,  $T_{\text{July}}$ ,  $P_{\text{ann}}$  were derived from WorldClim 2 version 2.1 (spatial resolution of 30  
163 seconds ( $\sim 1 \text{ km}^2$ ), <https://www.worldclim.org>; Fick and Hijmans, 2017) by extracting the climate data at  
164 the location of the modern sample sites using the *raster* package in R (version 3.5-11, Hijmans et al.,

165 2021; R Core Team, 2020). The WorldClim 2 dataset provides spatially interpolated gridded climate  
166 data aggregated from weather stations as temporal averages between 1970-2000 (Fick and Hijmans,  
167 2017). We used monthly average temperature data to extract the mean  $T_{July}$  and the “bioclimatic  
168 variables” bio1 ( $T_{ann}$ ) and bio12 ( $P_{ann}$ ).

169

## 170 **2.2 Reconstruction methods**

171 Our reconstruction approach included MAT (Overpeck et al., 1985) and WA-PLS (ter Braak and Juggins,  
172 1993) by applying the MAT and WAPLS functions from the *rioja* package (version 0.9-21, Juggins, 2019)  
173 for R (R Core Team, 2020) on our Northern Hemispheric fossil pollen synthesis. For each fossil location,  
174 we calculated the geographic distance between each modern sampling site and the fossil pollen record  
175 using the *rdist.earth* function from the *fields* R-package (version 10.3, Nychka et al., 2020) and selected  
176 a unique calibration set from modern sites within a 2000 km radius. We fixed the radius to 2000 km  
177 instead of 1500 km as suggested from a study in Eastern Asia by Cao et al. (2017), because the modern  
178 dataset density is rather low in Northern Asia. For the reconstruction with MAT, we used the original  
179 pollen percentages of the selected fossil pollen taxa, looking for 7 analogues between the pollen data  
180 and the selected calibration dataset. The dissimilarity between the fossil samples and the modern pollen  
181 assemblages was determined by squared-chord distance of the percentage data (Simpson, 2012; Cao  
182 et al., 2014).

183 In addition to the classic WA-PLS reconstruction, we also propose WA-PLS\_tailored. This approach  
184 addresses the problem that co-variation of climate variables today in space is transferred to the  
185 reconstruction even if the past temporal relationship among the climate variables mechanistically differs.  
186 In fact, this approach aims to make use of the full climate space covered by the modern pollen samples  
187 avoiding those samples in the calibration set that cause spatial covariation. This approach is based on  
188 the assumption that several climate variables can be reflected in one and the same pollen assemblage  
189 because different plant taxa have different optima in temperature and precipitation ranges and might  
190 therefore occur with different co-occurrence and abundance pattern. To reconstruct  $T_{July}$  we identified  
191 the  $P_{ann}$  range reconstructed by WA-PLS and extended it by 25% to both ends of the modern  $P_{ann}$  range  
192 in order to reduce the influence of  $P_{ann}$  on  $T_{ann}$  and  $T_{July}$  reconstruction due to co-variation. We applied  
193 the same method to the reconstruction of  $P_{ann}$ .  $T_{ann}$  and  $T_{July}$  were tailored by  $P_{ann}$ ;  $P_{ann}$  was tailored by

194  $T_{July}$  and, additionally, by  $T_{ann}$  (illustrated for an example in Appendix Fig. 24). Reconstruction  
195 uncertainties are provided as root mean square errors (RMSE) derived from the output in the MAT and  
196 WAPLS functions. Model errors of WA-PLS and MAT are reported as root mean square error of  
197 prediction (RMSEP) derived from leave-one-out cross-validation.

198 We provide site- or sample-specific measures of quality in addition to the error estimates and model  
199 statistics to allow the user to assess the quality of the climate reconstruction dataset. First, we applied  
200 a Canonical Correlation Analysis (CCA) to the modern training dataset in order to explore the modern  
201 relationship between the pollen spectra and the climate variables and to infer the explained variance in  
202 the modern pollen dataset by the target climate variables (ter Braak, 1988) by using the *cca* function in  
203 the *vegan* R-package (version 2.5-7, Oksanen et al., 2020). The ratio between constrained ( $\lambda_1$ ) and  
204 unconstrained ( $\lambda_2$ ) explained variance was determined for all modern training datasets used for climate  
205 reconstructions. High values of  $\lambda_1$  vs  $\lambda_2$  ( $\geq 1$ ) are commonly considered as an indicator to measure  
206 how well the target environmental variable is ~~strongly~~ related to the variation in the modern pollen data  
207 set (e.g. Juggins, 2013). However, most training data sets encompass multiple environmental variables  
208 that are often correlated and additional requirements to such variables would be necessary to explain a  
209 significant and independent portion of the variation in the training data set. While a careful design of the  
210 training data set can help reduce the effect of correlated environmental gradients, it can never eliminate  
211 them completely (Juggins, 2013). To infer the analogue quality as an indicator of no-analogue situations  
212 we calculated the minimum dissimilarity (squared chord distance) between modern pollen assemblages  
213 and fossil pollen assemblages with probability thresholds of 1% (indicating very good analogs), 2.5%  
214 (good analogs) and 5% (poor analogs) using the *minDC* function from the *analogue* R-package (version  
215 0.17-6, Simpson et al., 2021).

216 A statistical significance test (Telford and Birks, 2011) was applied using the *randomTF* function in the  
217 *palaeoSig* R-package (version 2.0-3, Telford, 2019). In this test, the proportion of variance in the fossil  
218 pollen data explained by the reconstructed environmental variable is estimated from redundancy  
219 analysis (RDA) and tested against a null distribution generated by replacing the modern training dataset  
220 from a total of 999 with randomly generated surrogate fields environmental variables from the training  
221 data. The surrogate fields were simulated to have realistic spatial autocorrelation As the modern training  
222 dataset is considered to include spatial autocorrelation we generated red noise datasets for temperature  
223 and precipitation by fitting variograms to the WorldClim 2 temperature and precipitation data. and



224 ~~running 1000-member ensembles were simulated~~ ~~tions for each variable. The datasets were added to~~  
225 ~~the random TF function as a new red noise null distribution.~~ A reconstruction is considered statistically  
226 significant if the reconstructed variable explains more of the variance than 95% of the random  
227 reconstructions (Telford and Birks, 2011). The reconstructed climate ~~variables~~ ~~parameters~~ were tested  
228 as introducing the environmental variable as a single variable in a run, as well as with partialling out the  
229 explained variance in the pollen data by the respective other variables.

230 We used Plantaginaceae (mostly representing *Plantago lanceolata*-type in Europe) and *Rumex*-type to  
231 assess human influence as an indicator for intense herding (Behre, 1988). In addition, we calculated the  
232 correlation between the WA-PLS reconstruction of  $T_{\text{July}}$ ,  $T_{\text{ann}}$  and  $P_{\text{ann}}$  and the pollen percentages of  
233 Plantaginaceae and *Rumex* for 9000, 3000 and 1000 years BP to assess potential biases in the dataset.

234

### 235 **3 Dataset description LegacyClimate 1.0: input data, reconstructions and reconstruction model** 236 **statistics**

237 LegacyClimate 1.0 provides pollen-based reconstructions and sample-specific reconstruction errors of  
238  $T_{\text{ann}}$ ,  $T_{\text{July}}$  and  $P_{\text{ann}}$  for 2594 fossil pollen records (i.e., a total of 146067 single pollen samples) from three  
239 reconstruction methods (WA-PLS, WA-PLS\_tailored, MAT). Furthermore, we provide the method-  
240 specific model metadata and quality measures for each record and each climate variable (Table 1). To  
241 ease data handling, the dataset files are separated into Western North America, Eastern North America,  
242 Europe and Asia.

243

244

245

246

247

248

249

250

251 **Table 1.** Structure and content of the LegacyClimate 1.0 data with details about the information  
 252 contained in the input datasets, in the climate reconstructions and the reconstruction model statistics.

| Datasets  | Content   |
|---|---|
| <b>Input datasets</b>                                     | Modern pollen dataset of 15379 sites  |
|   | Modern dataset of $T_{ann}$ , $T_{July}$ , $P_{ann}$  |
|   | Fossil pollen data (LegacyPollen 1.0) for 2594 sites with a total of 146067 samples   |
|   | Bacon age-depth models (LegacyAge 1.0) for 2579 sites   |
| <b>LegacyClimate 1.0: Climate reconstructions</b>         | Reconstructions and sample-specific reconstruction errors of $T_{ann}$ , $T_{July}$ and $P_{ann}$ for 25934 sites using MAT, WA-PLS and WA-PLS_tailored |
|   | Ensemble of 1000 realizations of the Bacon age-depth models for 2579 sites  |
| <b>LegacyClimate 1.0: Reconstruction model statistics</b> | <b>Site information</b> (Event label, Source, ID, Site name, Longitude, Latitude)   |
|   | <b>Modern pollen dataset information</b> (number of modern analogues, range of climate variables)   |

**Model statistics for each site for MAT, WA-PLS, WA-PLS\_tailored** (including  $r^2$  observed vs. predicted, RMSEP, no. of WA-PLS components)

---

**LegacyClimate 1.0: Quality Measures**

**Canonical Correlation Analysis (CCA)** of the modern training dataset

**Minimum dissimilarities** between modern pollen assemblages and fossil pollen assemblages for each record sample site for MAT

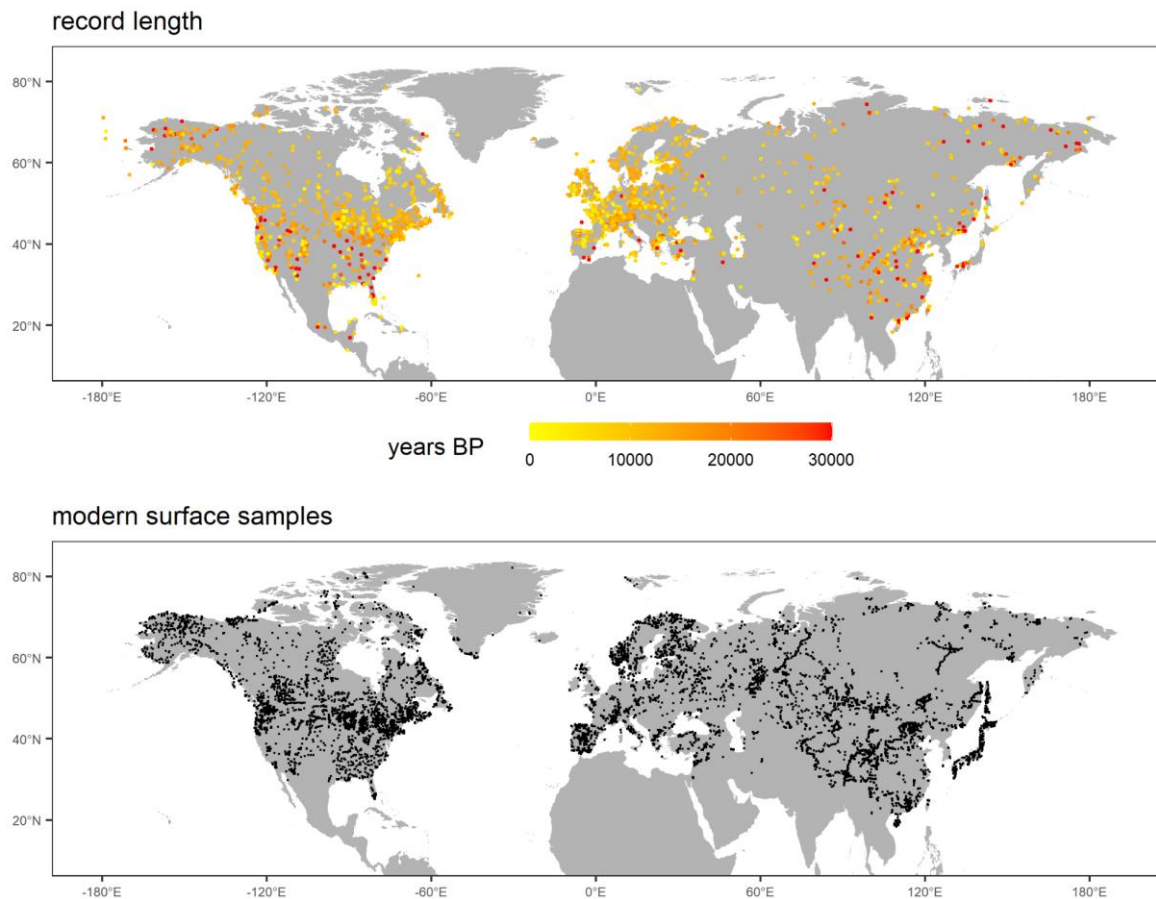
**Statistical significances** sensu Telford & Birks (2011) for each site for MAT, WA-PLS, WA-PLS\_tailored

---

253

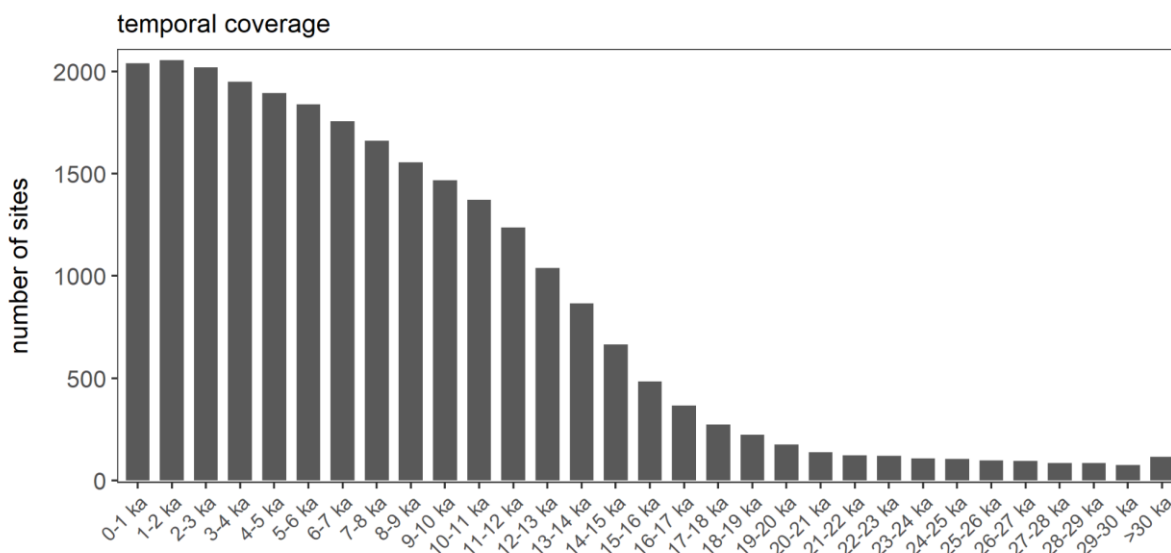
254 **4 Dataset assessment**255 **4.1 Spatial and temporal coverage of LegacyClimate 1.0**

256 In total, we provide reconstructions for 2594 fossil pollen records. Among them 670 records are located  
 257 infrom Eastern North America, 361 records infrom Western North America, 1075 records infrom Europe  
 258 and 488 Asian records (Fig. 1). Some few records are included that come from marine cores which were  
 259 taken from the continental shelf. They contain information from source areas from the nearby continents  
 260 (e.g. fluvially transported material). If users want to focus on terrestrial-only records, those marine sites  
 261 could be filtered out by the archive type provided in the metadata. Climate reconstructions for one fossil  
 262 record in the Western North American Dataset on Hawaii (Dataset-ID 17832, "Kealia Pond") could not  
 263 be performed as there were no modern training data available within a 2000 km area.  
 264 The temporal coverage of the records is rather uneven: 75 and 666 records cover the periods between  
 265 30-29 ka and 15-14ka, respectively (Fig. 2).



266

267 **Figure 1.** Upper panel<sup>Top</sup>: map indicating the spatial distribution and record lengths covered by the  
 268 LegacyPollen 1.0 dataset (Herzschuh et al., 2022c) for which climate reconstructions, temporal and  
 269 reconstruction uncertainties and reconstruction quality measures are provided in LegacyClimate 1.0 with  
 270 a total of 2594 records; Lower panel<sup>Bottom</sup>: spatial distribution of modern pollen dataset used for  
 271 reconstruction with a total of 15379 sites.



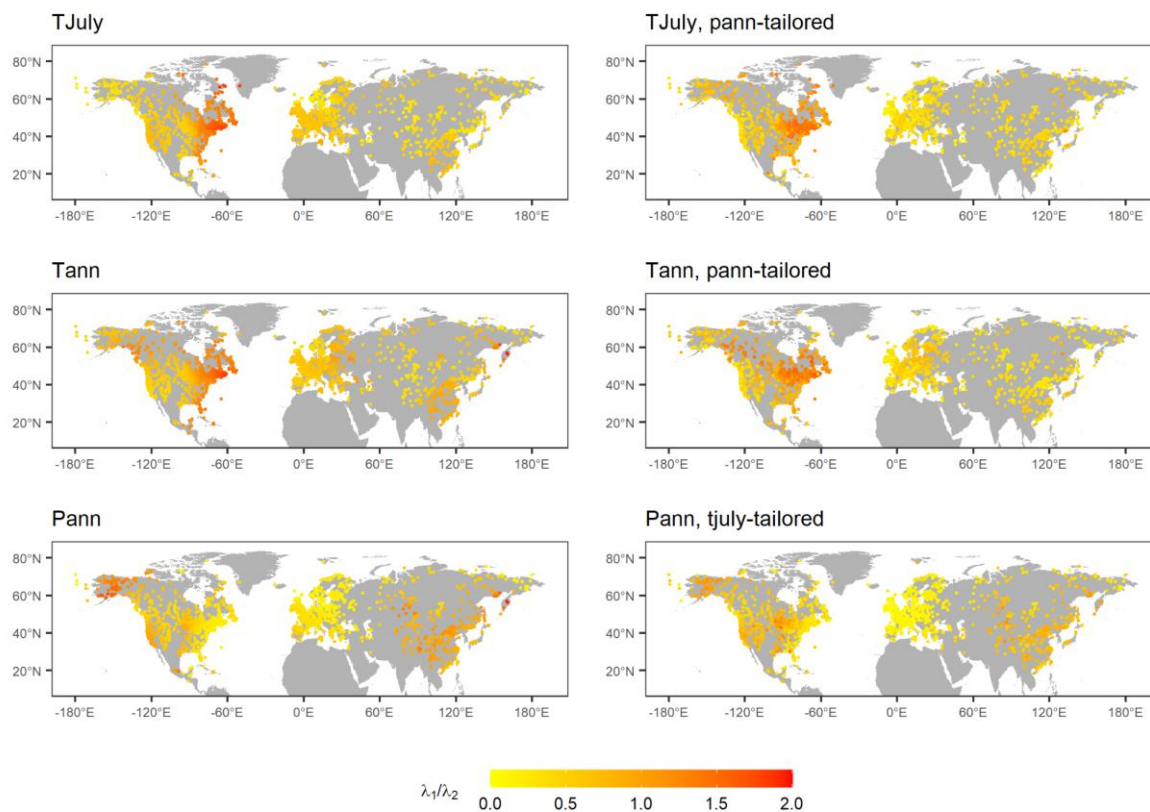
272

273 **Figure 2.** Number of records that cover certain millennia of the last 30 ka.

274

#### 275 **4.2 Modern relationships between pollen and climate assessed by constrained ordination.**

276 Results from CCA applied to modern datasets reveal that  $T_{July}$ -constrained ordinations have high  $\lambda_1/\lambda_2$   
 277 ratios, indicating a strong relationship between this climate variable and modern pollen assemblages, in  
 278 Eastern North America while low ratios can be found in Central Asia. The spatial pattern of  $\lambda_1/\lambda_2$  of  
 279 ordinations constrained by  $T_{ann}$  is overall similar to those of  $T_{July}$  but the ratios are slightly higher for  $T_{ann}$   
 280 than for  $T_{July}$ . Reconstructions for  $P_{ann}$  show low ratios in Europe and Eastern North America. Areas with  
 281 high ratios are concentrated in Alaska and East Asia (Fig. 3).



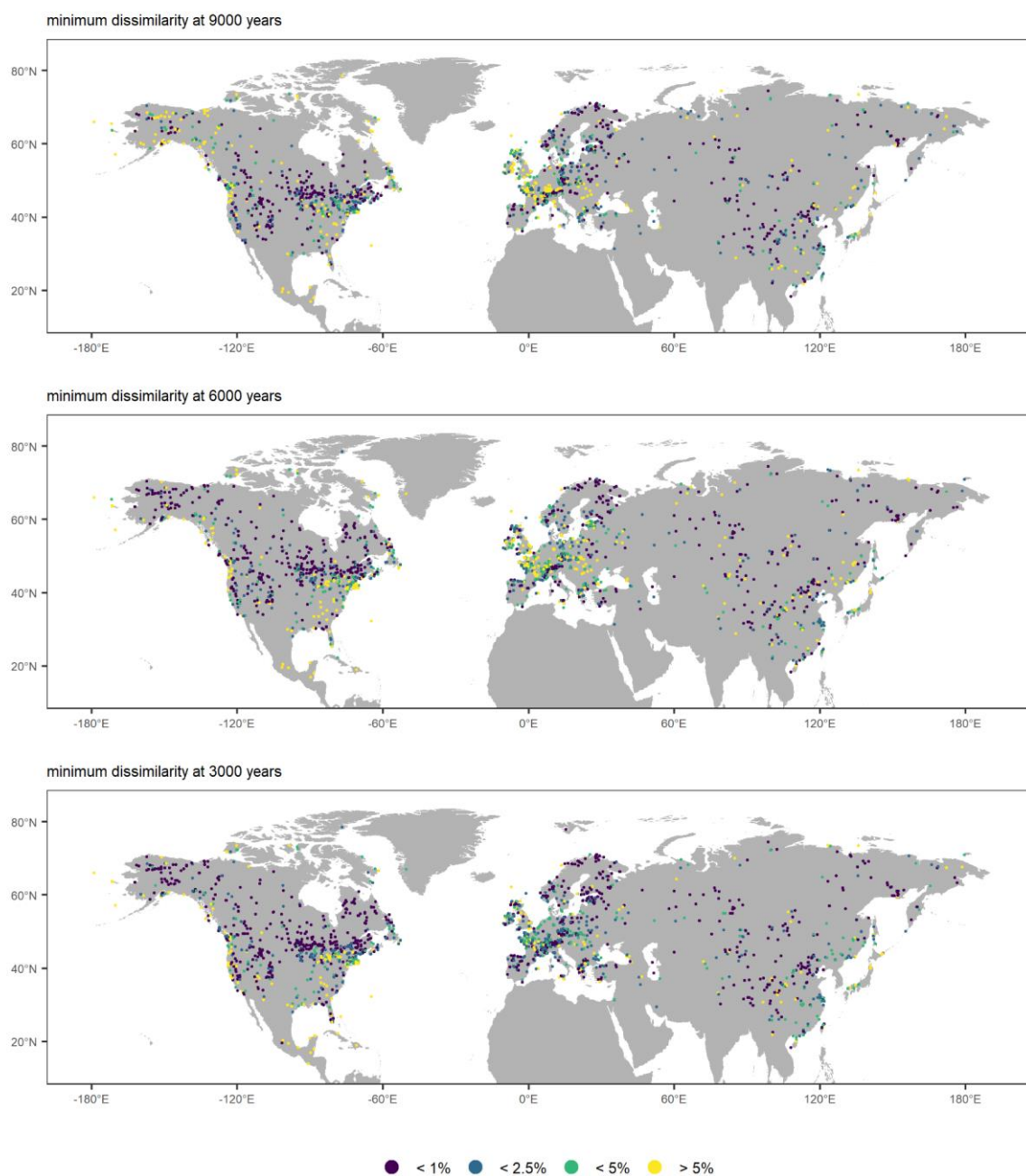
282  
 283 **Figure 3.** Maps showing  $\lambda_1/\lambda_2$ , representing the ratio of explained variance of first axis (constrained) vs.  
 284 second (unconstrained) axis as revealed by applying a CCA to all modern training datasets that were  
 285 used for the reconstructions. High ratios ( $\geq 1$ ) indicate a strong relationship between the modern pollen  
 286 datasets and climate and can be used to determine ecologically important determinants. Constraining  
 287 variables as well as tailoring of the dataset (see methods) is indicated in the map captions.

288

### 289 4.3 Analogue quality

290 The dissimilarity (squared chord distance) between modern pollen assemblages and fossil pollen  
 291 assemblages was calculated and extracted for distinct time-slices at 9000, 6000 and 3000 years BP. In  
 292 total, 36.4% (9000 years BP), 39.2% (6000 years BP) and 45.6% (3000 years BP) records indicate a  
 293 very good (<1%) analogue quality. The central part of the North American continent, Scandinavia and  
 294 Central Asia show a very good analogue quality for all time-slices investigated. Poor (<5%) analogues  
 295 can be found in Western Europe, the eastern parts of the United States and along the eastern Asian  
 296 coastline. Non-analogues (>5%) are found for 22.6% (9000 years BP), 20.47% (6000 years BP) and  
 297 12.5% (3000 years BP) record respectively, especially in Western Europe and at 9000 years BP in  
 298 Alaska (Fig. 4).

299



300

301 **Figure 4.** Analogue quality as assessed by squared chord distance between modern pollen  
 302 assemblages and fossil pollen assemblages. Results identify a very good (<1%), good (<2.5%) and poor  
 303 (<5%) analogues. Distances >5% are considered to indicate non-analogue situations (as percentage of  
 304 all distances among pollen samples in the modern dataset used for calibration).

305

306

307

#### 308 4.4 Prediction errors of LegacyClimate 1.0

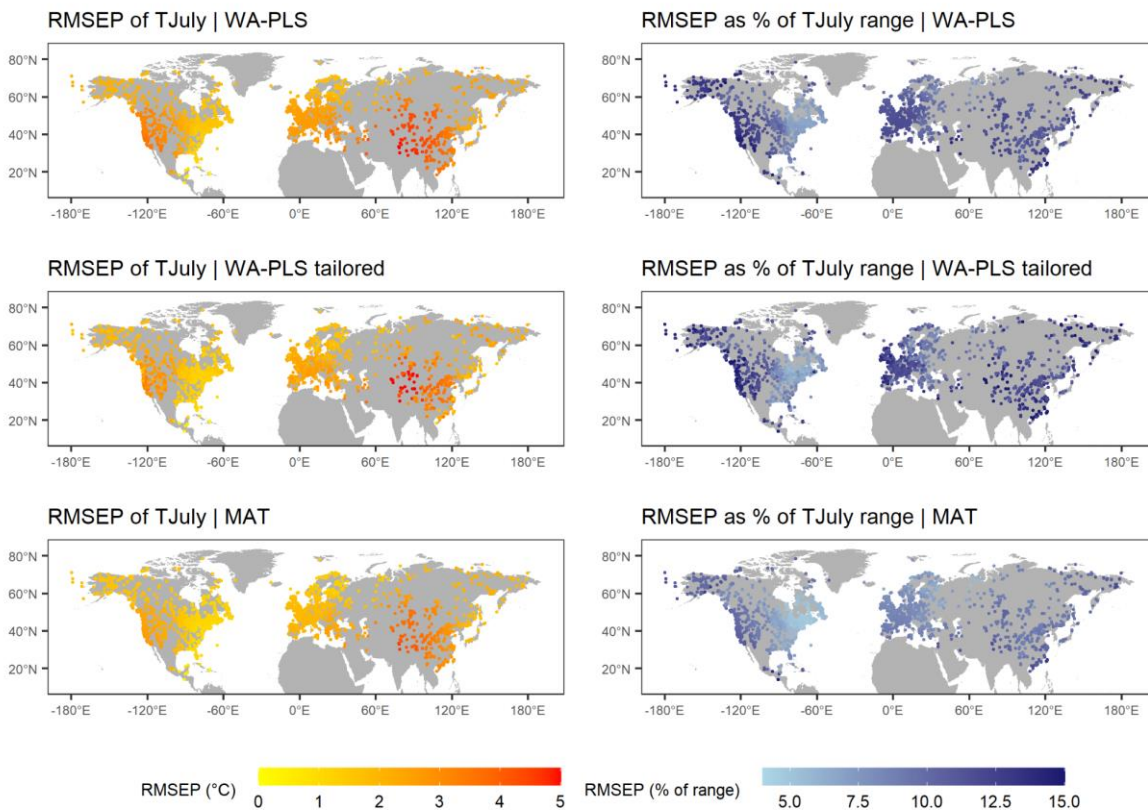
309 The mean RMSEPs and their standard deviations for  $T_{\text{ann}}$  are  $1.98 \pm 0.52^\circ\text{C}$  (MAT),  $2.61 \pm 0.53^\circ\text{C}$  (WA-  
310 PLS) and  $2.24 \pm 0.61^\circ\text{C}$  (WA-PLS\_tailored) and mean RMSEPs as a percentage of modern  $T_{\text{ann}}$  range  
311 are  $7.68 \pm 1.93\%$  (MAT),  $10.09 \pm 2.05\%$  (WA-PLS) and  $10.26 \pm 2.79\%$  (WA-PLS\_tailored). The largest  
312 mean RMSEP values are located in Central Asia in Kazakhstan, Mongolia and the north-western parts  
313 of the Tibetan Plateau and are consistent across all three reconstruction methods. Other areas with  
314 large mean RMSEP values are located in Western North America, Southern and Central Europe and  
315 south-east Asia. The smallest RMSEPs can be found along the east coast of North America. Relative  
316 to the modern temperature range, the RMSEP from this region also reveals the lowest fraction. In  
317 general, MAT has the lowest mean error fraction relative to the modern temperature range of all three  
318 methods.

319 The mean RMSEPs of  $T_{\text{July}}$  are  $1.90 \pm 0.63^\circ\text{C}$  (MAT),  $2.50 \pm 0.73^\circ\text{C}$  (WA-PLS) and  $2.21 \pm 0.75^\circ\text{C}$  (WA-  
320 PLS\_tailored) and mean percentages of  $T_{\text{July}}$  range are  $8.11 \pm 1.64\%$  (MAT),  $10.71 \pm 1.94\%$  (WA-PLS)  
321 and  $10.70 \pm 2.60\%$  (WA-PLS\_tailored). Thus, they are slightly smaller than those of  $T_{\text{ann}}$  but slightly larger  
322 as a percentage of the range. The spatial patterns, however, are largely similar to those of  $T_{\text{ann}}$ .

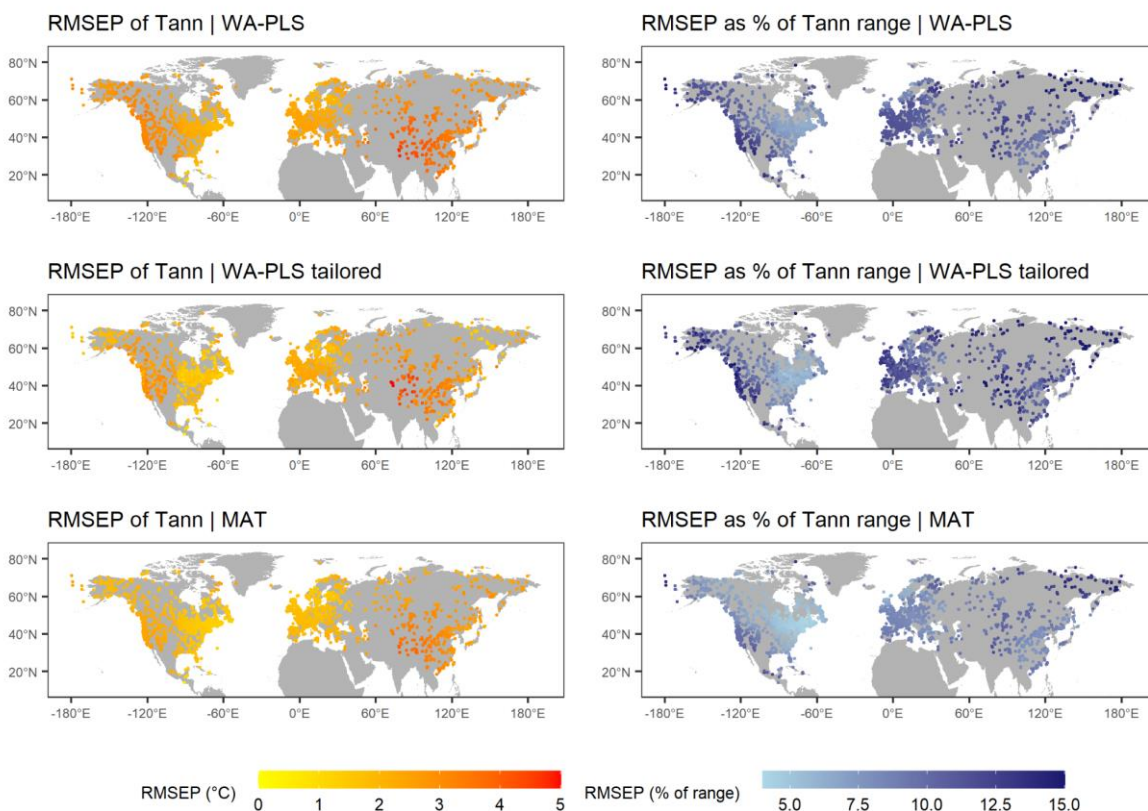
323 The mean RMSEPs of  $P_{\text{ann}}$  are  $176.38 \pm 51.40$  mm (MAT),  $244.48 \pm 75.84$  mm (WA-PLS) and  
324  $232.71 \pm 98.57$  mm (WA-PLS\_tailored) and mean percentages of  $P_{\text{ann}}$  range are  $6.78 \pm 1.48\%$  (MAT),  
325  $9.27 \pm 1.70\%$  (WA-PLS) and  $10.26 \pm 2.67\%$  (WA-PLS\_tailored). High RMSEPs are found for Western  
326 North America, Europe and along the coastline of south-east Asia, while the lowest RMSEP values are  
327 found for Central Asia. A clear division in RMSEPs are found on the North American continent: while  
328 the western part of North America (with the exception of Alaska) has a rather high RMSEP, the eastern  
329 part of North America has a smaller RMSEP. This pattern is found for all three methods (Fig. 5).

330

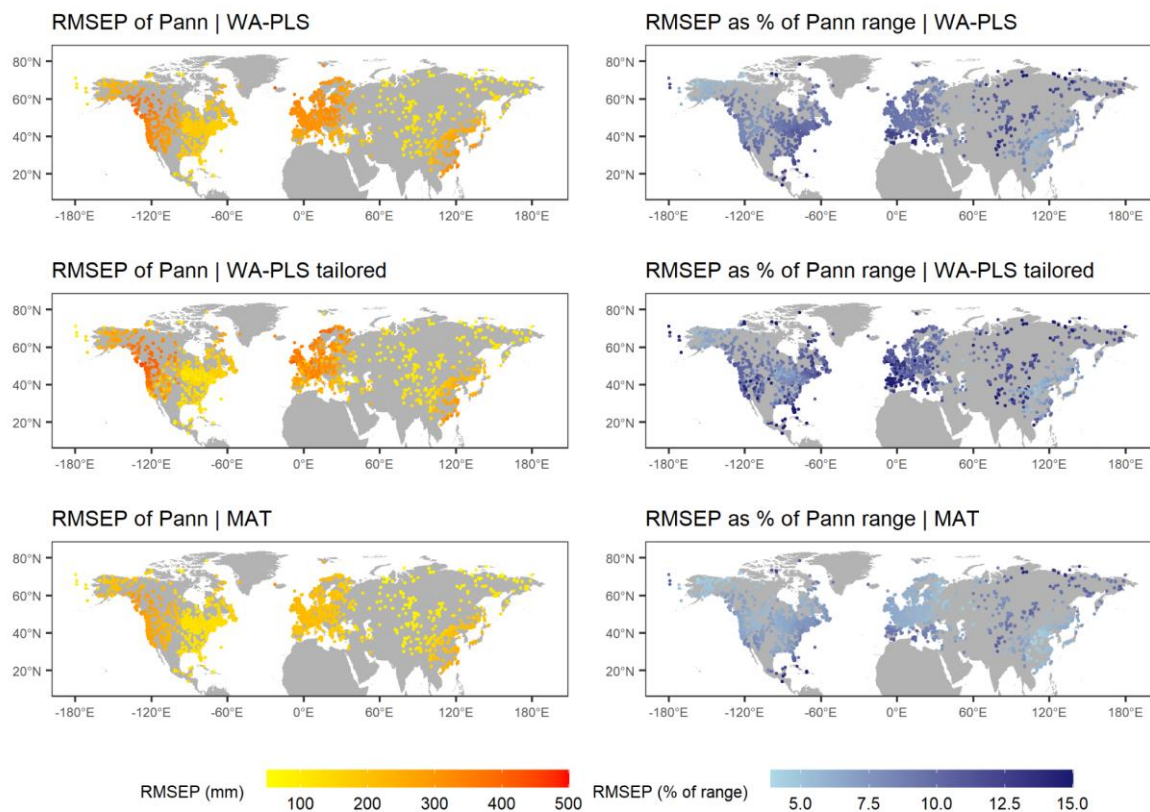




331



332



333

334 **Figure 5.** Spatial distribution of root-mean-squared error of prediction (RMSEP) as inferred from leave-  
 335 one-out cross-validation presented as absolute values and as a percentage of the range of mean July  
 336 temperature ( $T_{\text{July}}$ ), mean annual temperature ( $T_{\text{ann}}$ ), annual precipitation ( $P_{\text{ann}}$ ) in the modern pollen  
 337 data used for reconstruction for the three methods applied (Weighted-Averaging Partial-Least Squares  
 338 regression (WA-PLS), WA-PLS using a training set from within a limited climate range (WA-  
 339 PLS\_tailored) and Modern Analogue Technique (MAT)).

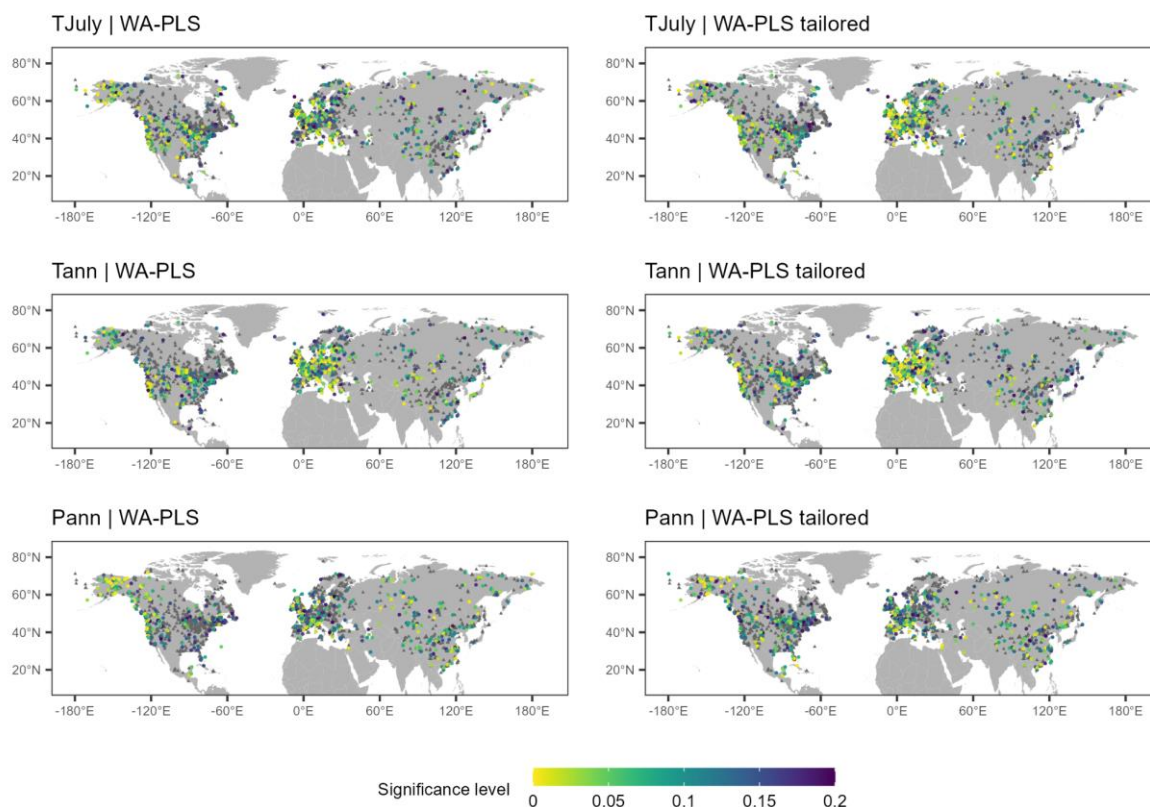
340

#### 341 4.5 Significance test

342 A significance test ( $p < 0.1$  and in addition  $p < 0.2$ , see methods) according to Telford and Birks (2011)  
 343 was performed for each record (Fig. 6; Table 2). For the  $T_{\text{July}}$  reconstruction, 16.4% [ $p < 0.2$ : 27.2%]  
 344 30.9% (WA-PLS) and 19.0% [ $p < 0.2$ : 29.1%] 35.2% (WA-PLS\_tailored) of all records passed the  
 345 significance test when included as a single variable in the significance test. Partialling out precipitation  
 346 as a conditional variable causes an increase in the amount of significant records to 19.0% [ $p < 0.2$ : 30.6%]  
 347 35.5% for WA-PLS of  $T_{\text{July}}$ , but a decrease for WA-PLS\_tailored to 16.7% [ $p < 0.2$ : 27.6%] 33.6% of all  
 348 records. The  $T_{\text{ann}}$  reconstruction is significant for 16.5% [ $p < 0.2$ : 27.1%] 32.8% (WA-PLS) and 20.0%  
 349 [ $p < 0.2$ : 31.6%] 36.1% (WA-PLS\_tailored) of all records when tested as a single variable. When

350 partialling out precipitation, the amount of significant records slightly indecreases for both-WA-PLS, but  
 351 decreases for-and WA-PLS\_tailored. 13.0% [p<0.2: 21.8%] 32.4% (WA-PLS) and 14.3% [p<0.2: 25.4%]  
 352 33.4% (WA-PLS\_tailored) of all records pass the significance test when testing  $P_{ann}$  as a single variable.  
 353 In contrast to the significance tests for  $T_{ann}$ , pPartialling out the mean July temperature as a conditional  
 354 variable increases the number of significant records for both WA-PLS and WA-PLS\_tailored.

355



356

357 **Figure 6.** Maps showing mean July temperature ( $T_{July}$ ), mean annual temperature ( $T_{ann}$ ), annual  
 358 precipitation ( $P_{ann}$ ) records that passed the reconstruction significance test ( $p < 0.24$ ). Colors  
 359 indicate~~indicates~~ the significance level. Records that did not pass the significance level ( $p \geq 0.2$ ) are  
 360 shown as grey rectangles.

361

362

363

364

365 **Table 2.** Percentage of records that pass the reconstruction significance test ( $p < 0.1$  and  $p < 0.2$ ) sensu  
 366 Telford and Birks (2011). The values in brackets for  $p < 0.1$  indicate the significance values without taking  
 367 spatial autocorrelation into account.

|  | WA-PLS                  |              | WA-PLS_tailored         |              | MAT                     |              |
|--|-------------------------|--------------|-------------------------|--------------|-------------------------|--------------|
|  | $p < 0.1$               | $p < 0.2$    | $p < 0.1$               | $p < 0.2$    | $p < 0.1$               | $p < 0.2$    |
| T <sub>July</sub>  | <u>16.4%</u><br>(30.9%) | <u>27.2%</u> | <u>19.0%</u><br>(35.2%) | <u>29.1%</u> | <u>44.1%</u><br>(42.4%) | <u>56.8%</u> |
| T <sub>July</sub><br>partialling<br>out P <sub>ann</sub> | <u>19.0%</u><br>(35.5%) | <u>30.6%</u> | <u>16.7%</u><br>(33.6%) | <u>27.6%</u> | <u>48.7%</u><br>(39.9%) | <u>61.4%</u> |
| T <sub>ann</sub>   | <u>16.5%</u><br>(32.8%) | <u>27.1%</u> | <u>20.0%</u><br>(36.1%) | <u>31.6%</u> | <u>46.5%</u><br>(42.4%) | <u>57.7%</u> |
| T <sub>ann</sub><br>partialling<br>out P <sub>ann</sub>  | <u>16.7%</u><br>(32.6%) | <u>27.1%</u> | <u>18.4%</u><br>(34.1%) | <u>28.8%</u> | <u>48.1%</u><br>(39.2%) | <u>61.9%</u> |
| P <sub>ann</sub>   | <u>13.0%</u><br>(32.1%) | <u>21.8%</u> | <u>14.3%</u><br>(33.4%) | <u>25.4%</u> | <u>36.5%</u><br>(36.3%) | <u>51.1%</u> |
| P <sub>ann</sub><br>partialling<br>out T <sub>July</sub> | <u>14.5%</u><br>(34.2%) | <u>24.1%</u> | <u>16.5%</u><br>(36.5%) | <u>28.2%</u> | <u>39.4%</u><br>(34.5%) | <u>53.7%</u> |

368

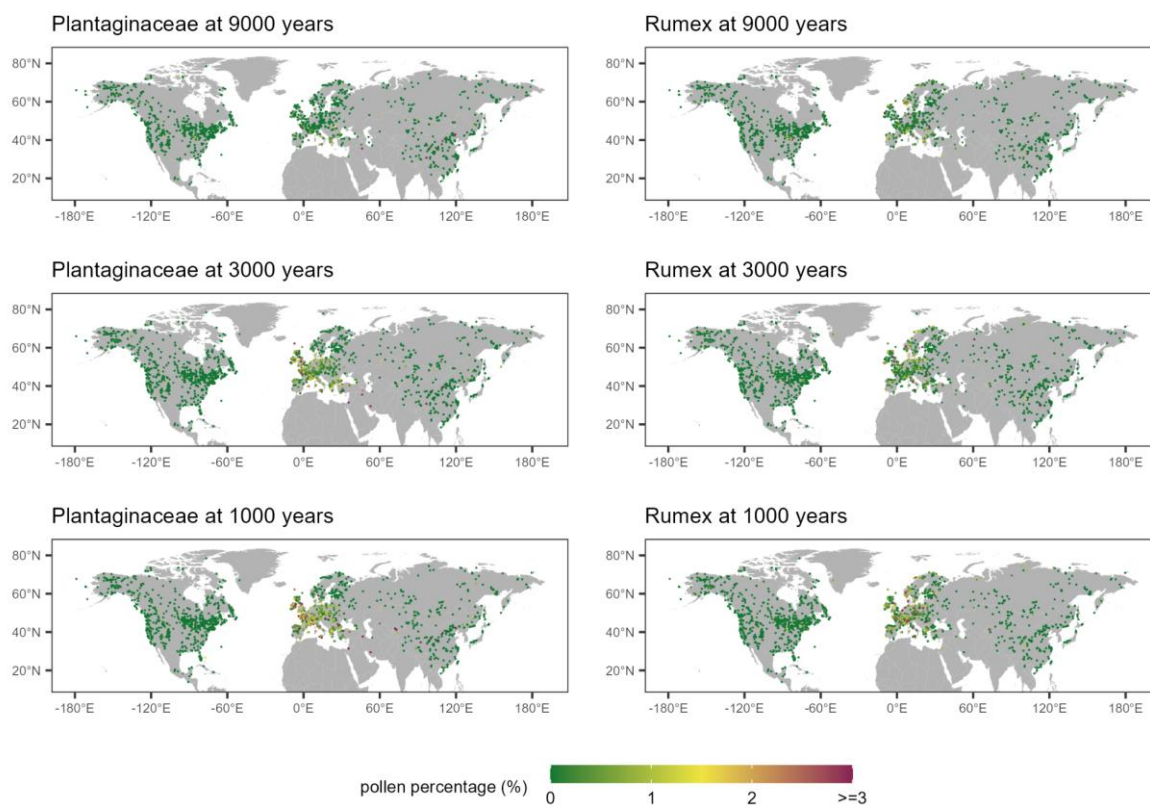
369

370

#### 371 4.6 Human impact

372 We used the abundance of Plantaginaceae and *Rumex* as indicators of grazing and such intense animal  
 373 husbandry. Overall weak human impact is inferred for North America and Northern Asia. The indicators  
 374 show indicate strong human impact only in individual single records at 9000 years BP in China and the  
 375 Mediterranean region (Fig. 7). The percentage values of Plantaginaceae and *Rumex* were high  
 376 especially in Europe for 3000 years and 1000 years BP which indicates growing human impact on that  
 377 region. High Plantaginaceae correlate with low  $T_{July}$  and high  $P_{ann}$  in Central Europe indicating potential  
 378 biases in the temperature reconstructions i.e. too low temperatures become reconstructed. Similar  
 379 correlations are found for Rumex, especially in Northern Europe (Fig. 8).

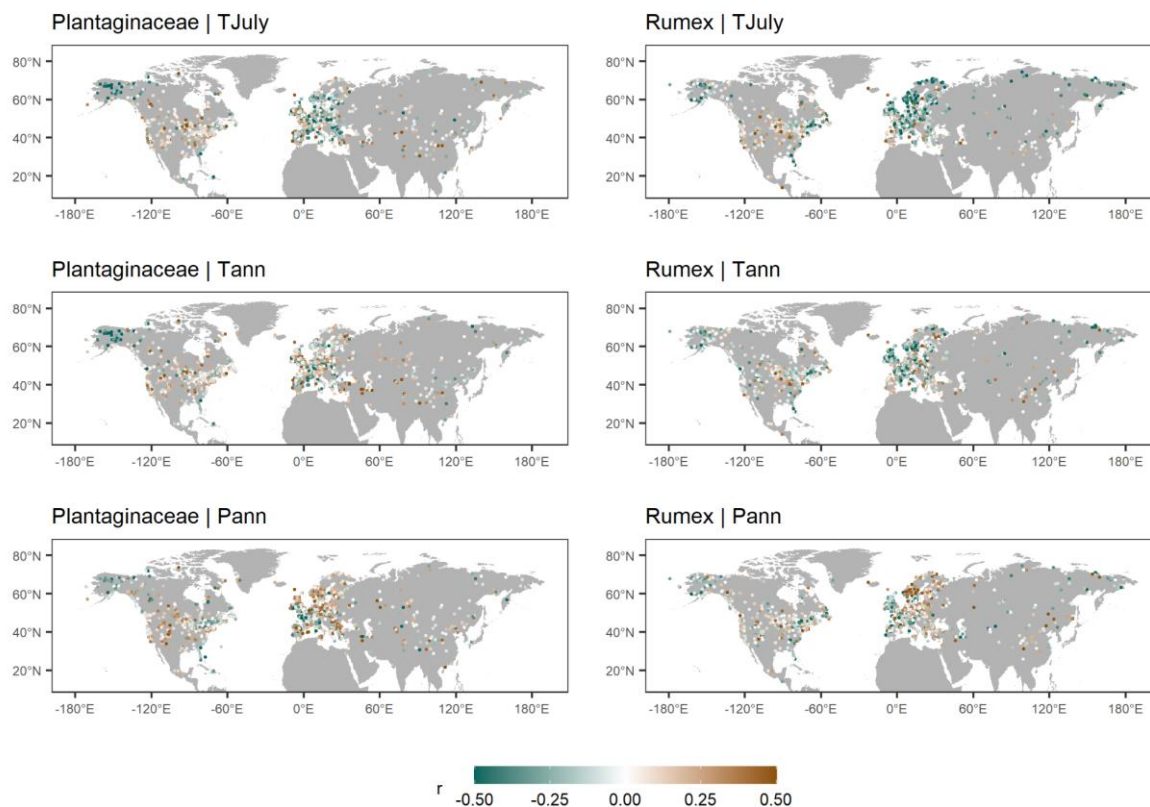
380



381

382 **Figure 7.** Abundance of Plantaginaceae (left) and *Rumex* (right) at 9000, 3000 and 1000 years BP.

383 Colors indicate percentage values.



384

385 **Figure 8.** Correlation between the percentage of Plantaginaceae (left) and *Rumex* (right) and  
 386 reconstructed  $T_{July}$ ,  $T_{ann}$  and  $P_{ann}$  with WA-PLS.

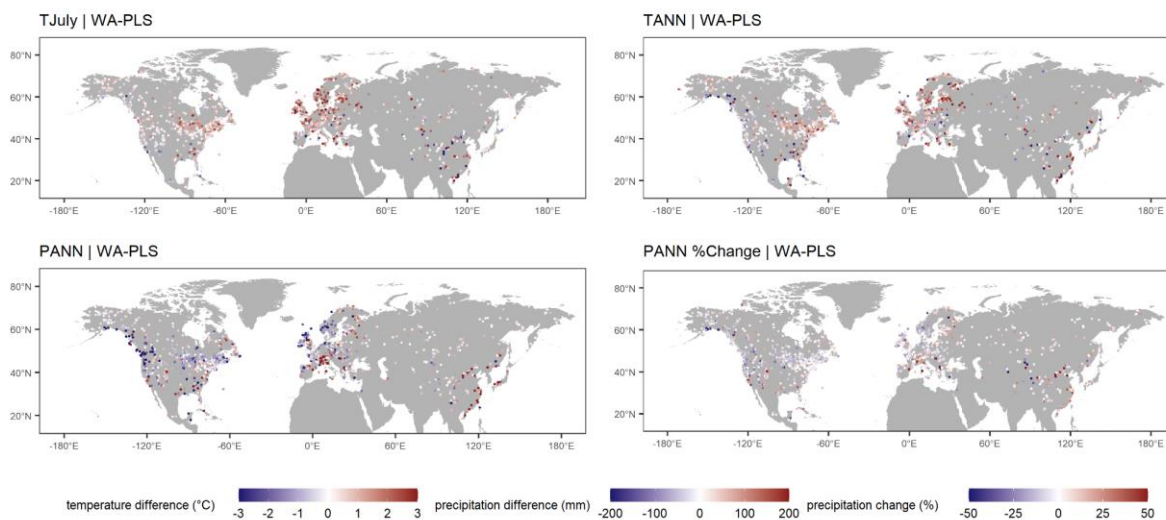
387

#### 388 4.7 Assessment of major temporal patterns of LegacyClimate 1.0

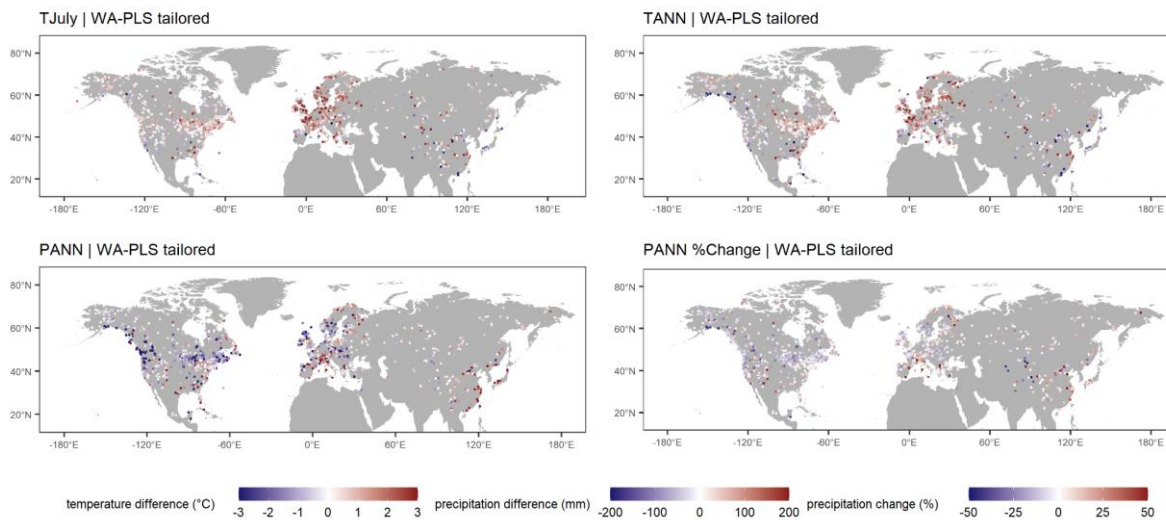
389 To illustrate the difference between Mid- and Late Holocene climate, we calculated the value for the  
 390 three climate variables at 6 ka BP and 1 ka BP, each time taking the average of the interpolated values  
 391 at those ages for the ensemble of 1000 realizations of the age-depth models (Li et al., 2022). Differences  
 392 between these time-slices reveal warmer and drier conditions during the Mid-Holocene compared with  
 393 Late Holocene conditions, especially in Eastern North America, but also in Central and Northern Europe.  
 394 The overall patterns are in good agreement for all three methods but show differences on a regional  
 395 scale, especially when comparing the reconstructions with WA-PLS and MAT. For  $T_{July}$ , the  
 396 reconstruction with MAT shows greater temperature differences in Western North America and south-  
 397 east Asia. Compared to the reconstruction with WA-PLS, there is a reduced cooling from 6 ka to 1 ka in  
 398 Eastern Europe and a warming instead of a cooling in the Western Mediterranean region and along the  
 399 south-eastern Asian coastline in MAT. For large areas in North America and Europe, the reconstructions  
 400 with WA-PLS suggest an increase in precipitation from 6 to 1 ka BP. A shift to drier conditions can be

401 found along the south-eastern coastline in North America, in the Mediterranean Region and especially  
402 in south-east Asia. The reconstruction with MAT reveals a gradient from increasing precipitation in  
403 south-western Europe to decreasing precipitation in north-eastern Europe. In contrast to the  
404 reconstructions with WA-PLS, records along the south-eastern Asian coastline suggest an increase in  
405 precipitation with MAT rather than a decrease (Fig. 9).

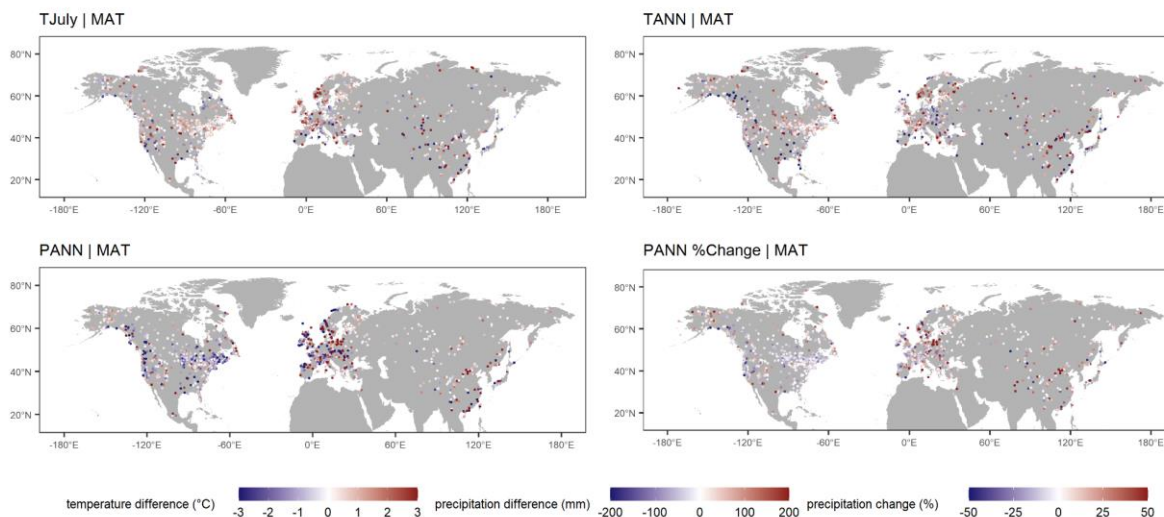
406



407

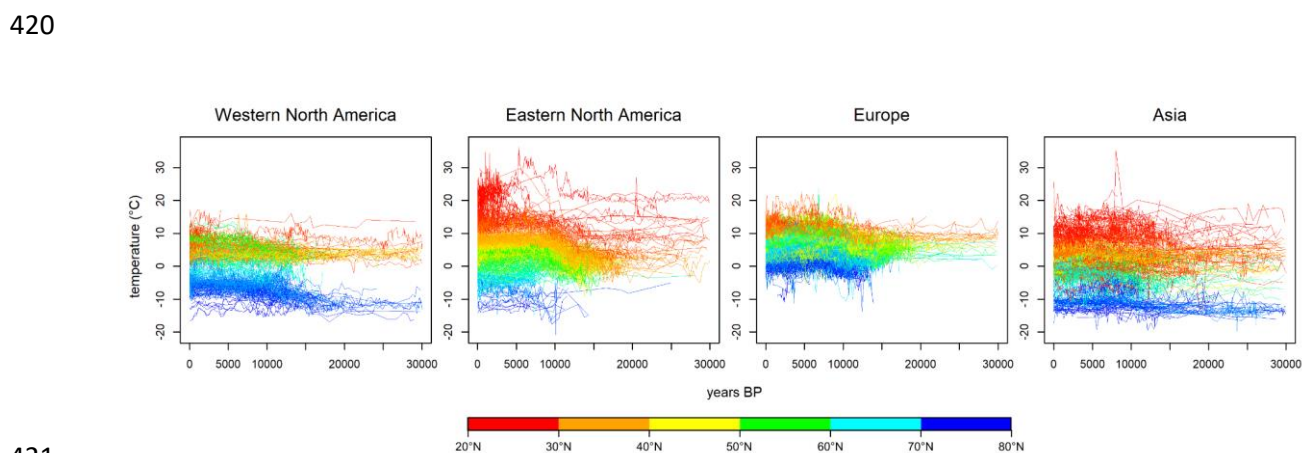


408



409  
 410 **Figure 9.** Difference from 6 ka to 1 ka for mean July temperature ( $T_{July}$ ), mean annual temperature ( $T_{ann}$ ),  
 411 annual precipitation ( $P_{ann}$ ) and  $P_{ann}\%$  as reconstructed from WA-PLS (upper panel), WA-PLS\_tailored  
 412 (middle panel) and MAT (lower panel).

413  
 414 Time-series of absolute  $T_{ann}$  reconstructions reveal temporal as well as latitudinal spatial variation on  
 415 the single continents. Eastern North America and Asia show the most variation in the low latitudes. It is  
 416 also Eastern North America which shows the most pronounced latitudinal gradient. In Western North  
 417 America, the most variation takes place in the high latitudes, while the variation is concentrated to the  
 418 mid-latitudes in Europe. Especially in North America, the warming since the last deglaciation and the  
 419 beginning of the Holocene is well shown in the temporal variation of the time-series (Fig. 10).



421  
 422 **Figure 10.** Time-series of absolute mean annual temperature ( $T_{ann}$ ) reconstruction with WA-PLS for  
 423 each (sub-)continent. Colors denote the latitude of record origin. Age and reconstruction uncertainties  
 424 are not plotted but are available for each time-series.



425

426 **4.8 Assessment of consistency among reconstruction methods**

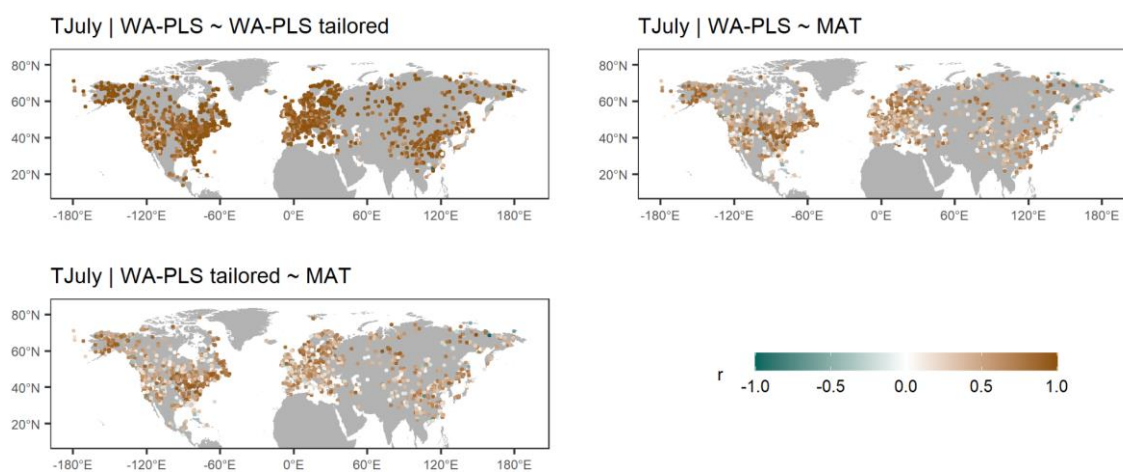
427 Reconstructions with MAT are, in general, in good agreement with those derived from the WA-PLS.

428 Comparing MAT with WA-PLS, 37.3% ( $T_{July}$ ), 38.9% ( $T_{ann}$ ) and 30.4% ( $P_{ann}$ ) of all records have a positive429 correlation of  $r \geq 0.6$ . Strong positive correlations ( $r \geq 0.9$ ) can mainly be identified in Eastern North

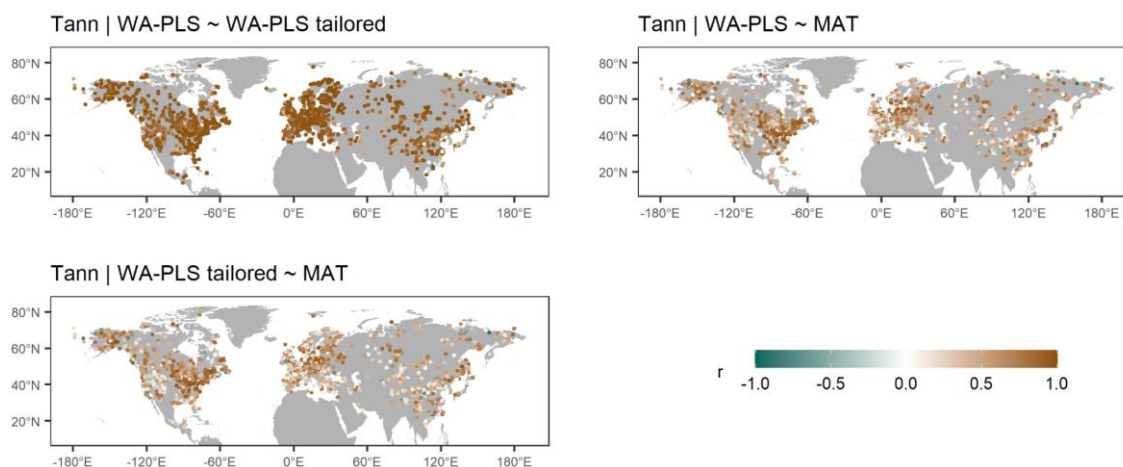
430 America, while weak correlation can be found for large areas in central North America and most of

431 Europe (Fig. 11).

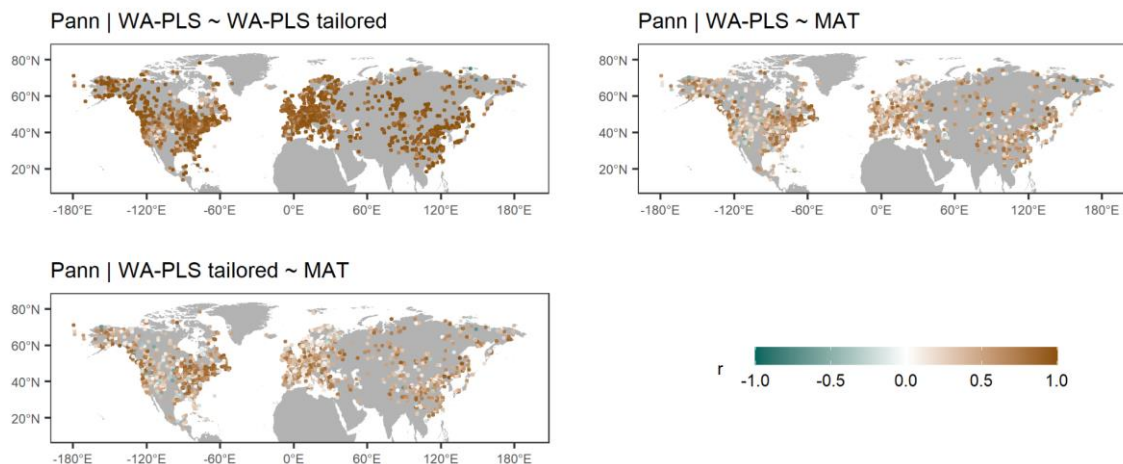
432



433



434



435  
 436 **Figure 11.** Correlation between time-series of the 3 different reconstruction methods used - weighted-  
 437 averaging partial least squares using a global training set (WA-PLS), WA-PLS using a training set with  
 438 a limited modern climate range (WA-PLS\_tailored) and the modern analogue technique (MAT) for the  
 439 three climate variables of mean July temperature ( $T_{July}$ ), mean annual temperature ( $T_{ann}$ ) and annual  
 440 precipitation ( $P_{ann}$ ).

441  
 442 WA-PLS\_tailored used a reduced modern training dataset (illustrated for an example in Appendix Fig.  
 443 [24](#)). The tailoring successfully reduced the co-variation of temperature and precipitation in the modern  
 444 dataset as indicated by the distribution of the correlation coefficient in Fig. 12. Nevertheless, the obtained  
 445 reconstructions are largely consistent between WA-PLS and WA-PLS-tailored: a correlation of  $r \geq 0.9$   
 446 is found for 59.2% of all records for  $T_{July}$ , 60.7% for  $T_{ann}$  and 56.5% for  $P_{ann}$ .



447  
 448 **Figure 12.** Violin plot of the correlation coefficients between  $T_{\text{July}}$  and  $P_{\text{ann}}$  in the 15379 training datasets  
 449 used for the reconstructions. Left: used for WA-PLS reconstructions; middle: WA-PLS  $T_{\text{July}}$ -tailored  
 450 (used for the reconstruction of  $P_{\text{ann}}$ ); WA-PLS  $P_{\text{ann}}$ -tailored (used for the reconstruction of  $T_{\text{July}}$ ).

451

## 452 5 Discussion

### 453 5.1 Impact of the fossil pollen data source on LegacyClimate 1.0 quality

454 LegacyClimate 1.0 contains reconstructions of climate variables from fossil pollen data derived from  
 455 open-access data repositories. The fossil records were derived from multiple natural archives, most  
 456 commonly, assemblages from continuous lacustrine and peat accumulations (Herzschuh et al., 2022c).  
 457 Different sizes of lakes and peat areas result in varying sizes of pollen source areas and thus the spatial  
 458 representativeness of a record. ~~While~~ While small lakes and peatlands are considered to provide information  
 459 about the (extra-)local scale, ~~while~~ the regional signal is better represented in pollen assemblages from  
 460 large lakes (Jackson, 1990; Sugita, 1993). However, taphonomic changes of the records originating, for  
 461 example, from lake level changes may impact the reconstructed climate. Pollen from azonal riverine  
 462 vegetation might be over-represented in fluvially impacted pollen records.

463 Our dataset is based on taxonomically harmonized modern and fossil pollen datasets using a restricted  
 464 number of taxa. Such an approach guarantees that all records are handled consistently. Although losing  
 465 taxonomic information when merging taxa together into a higher taxonomic level, it also increases the

466 possibility of matching climate analogues in the modern and the fossil datasets. However, one needs to  
467 keep in mind that species with different ecological requirements may be merged together into one genus  
468 or family, for example, *Pinus* species that are restricted to tropical or subtropical areas in China or ones  
469 that grow in boreal forests (Cao et al., 2013; Tian et al., 2017).

470 Along with the pollen assemblages, data repositories also provide chronological information for fossil  
471 records. The quality of such chronologies varies strongly with respect to dating methods, calibration and  
472 numerical algorithms for determining an age-depth relationship (Blois et al., 2011; Trachsel and Telford,  
473 2017). Having accurate and precise chronologies is thus of pivotal importance for reconstructing past  
474 climate in order to identify temporo-spatial patterns and therefore in helping to evaluate climate model  
475 outputs. The advantage of the fossil pollen dataset used for the reconstruction presented here (i.e.,  
476 LegacyPollen 1.0; Herzschuh et al., 2022c) is that it has harmonized chronologies (LegacyAge 1.0)  
477 along with information about uncertainties as well as related metadata and scripts that allow a  
478 customized re-establishment of the chronologies (Li et al., 2022). Accordingly, we were able to provide  
479 sample specific age-uncertainties along with reconstruction uncertainties.

480

## 481 5.2 Modern pollen and climate data sources and LegacyClimate 1.0 quality

482 We a priori selected  $T_{July}$ ,  $T_{ann}$  and  $P_{ann}$  as target variables for our reconstructions. However, we provide  
483  $\lambda_1/\lambda_2$  (i.e. explained variance of the climate variable in the modern pollen data set relative to the variance  
484 explained by the unconstrained first axis; ter Braak, 1988), a commonly used proxy for the assessment  
485 of reconstructions. The higher  $\lambda_1/\lambda_2$  in the spatial modern dataset the higher the chance that this target  
486 climate variable has also impacted vegetation over time and is thus reflected in the variation of the fossil  
487 pollen dataset. As a rule of thumb, a ratio of 1 is considered to indicate reliable reconstructions (Juggins,  
488 2013) though useful reconstructions may also be obtained from datasets with lower values. As expected,  
489 maps of RMSEPs reveal similar spatial pattern as the results of constrained ordination. Our results  
490 indicate that in particular calibration sets from Europe have low ratios and a high RMSEP for all climate  
491 variables (despite having a high number of modern samples), likely related to the human impact on the  
492 modern and fossil data. Some areas that are known for its sensitivity to precipitation e.g. Eastern Asia  
493 show low RMSEPs as expected for  $P_{ann}$  but on the other hand show a low sensitivity to  $T_{ann}$  and  $T_{July}$ .

494 For our study we used the, to our knowledge, largest modern dataset ever used in a pollen-based climate  
 495 reconstruction. For fossil pollen records in areas with an insufficient coverage of modern surface pollen  
 496 samples (e.g., Central Asia or Western Siberia), it might be difficult to create a calibration dataset that  
 497 maps the required variety of environmental and climatic gradients and therefore find enough modern  
 498 analogues for reconstructions with a classification approach such as MAT. This is indicated by the high  
 499 RMSEPs as percentages of gradient length in these areas. Our routine uses the modern pollen data  
 500 from within a radius of 2000 km around the site of the fossil record. The information provided in the  
 501 reconstruction metadata including number of modern pollen samples and ranges of reconstructed  
 502 variables, allow an assessment of the modern dataset used for reconstruction. Our assessments of the  
 503 modern dataset (e.g. using CCA), the transfer function (e.g. RMSEP) and the reconstruction (e.g. the  
 504 significance test) revealed also the potential biases in the pollen-based reconstruction and pointed to  
 505 limitations. Further validation and assessments of the results and more comprehensive uncertainty  
 506 analyses e.g. by applying forward modelling approaches (Izumi & Bartlein, 2016; Parnell et al., 2016)  
 507 would be highly valuable.

508 ~~We a priori selected  $T_{July}$ ,  $T_{ann}$  and  $P_{ann}$  as target variables for our reconstructions. However, we provide~~  
 509  ~~$\lambda_1/\lambda_2$  (i.e. explained variance of the climate variable in the modern pollen data set relative to the variance~~  
 510 ~~explained by the unconstrained first axis; ter Braak, 1988), a commonly used proxy for the assessment~~  
 511 ~~of reconstructions. The higher  $\lambda_1/\lambda_2$  in the spatial modern dataset the higher the chance that this target~~  
 512 ~~climate variable has also impacted vegetation over time and is thus reflected in the variation of the fossil~~  
 513 ~~pollen dataset. As a rule of thumb, a ratio of 1 is considered to indicate reliable reconstructions (Juggins,~~  
 514 ~~2012) though useful reconstruction may also be obtained from datasets with lower values. As expected,~~  
 515 ~~maps of RMSEPs reveal similar spatial pattern as the results of constrained ordination. Our results~~  
 516 ~~indicate that in particular calibration sets from Europe have low ratios and a high RMSEP for all climate~~  
 517 ~~variables (despite we have a high number of modern samples), likely related to the human impact on~~  
 518 ~~the modern and fossil data. Some areas that are known for its sensitivity to precipitation e.g. Eastern~~  
 519 ~~Asia show low RMSEPs as expected for  $P_{ann}$  but on the other hand show a low sensitivity to  $T_{ann}$  and~~  
 520  ~~$T_{July}$ .~~

521

522

523

### 524 **5.3 Reconstruction method and LegacyClimate 1.0 quality**

525 Overall, the three reconstruction approaches, MAT, WA-PLS and WA-PLS\_tailored yield rather similar  
526 results i.e. indicated by the overall high correlation between the reconstructions of the different methods  
527 (Fig. 11). Accordingly, the major trends at global or continental scales are similar, even if the actual  
528 amplitude of change may vary locally. As each method has its own strengths and weaknesses, there is  
529 not one set of reconstructions that is absolutely superior. One advantage of our multi-method  
530 reconstruction dataset is that users can identify the methods that are likely to perform best in a selected  
531 region and/or specific reconstructions. MAT is often recommended for large-scale studies, but it is highly  
532 sensitive to the quality of analogues (Chevalier et al. 2020). Low analogue situations can arise from two  
533 causes: climate conditions that differ strongly from today (e.g., the low atmospheric CO<sub>2</sub> concentration  
534 during the LGM; Jackson and Williams, 2004), or in regions with limited modern samples (e.g.,  
535 extratropical Asia). Furthermore, growing human influence on the landscape since the Middle to Late  
536 Holocene especially in densely settled regions in Europe contributed to gaps within the potential  
537 bioclimatic space of taxa and probably also led to extinction events, especially for disturbance-  
538 dependent taxa (Zanon et al., 2018). We report the analogue distance for each sample to help identify  
539 such situations. From our assessments, we revealed that analogues quality is overall rather good at  
540 least for the Holocene and except for Western Europe in particularly the British Isles (Fig. 4).

541 In contrast to MAT, WA-PLS (and most regression techniques in general) model relationships between  
542 pollen and climate and are, as such, less sensitive to the low analogue situations (Birks et al., 2010).  
543 They are, however, based on some modelling assumptions, such as the unimodality of the response of  
544 the pollen taxa to climate (ter Braak and Juggins 1993). This condition is not always met at the  
545 continental scale, primarily because of the limited taxonomic resolution of pollen data that merges  
546 several plant species with distinct climate requirements as one single pollen taxon. WA-PLS\_tailored  
547 has the same limitation but it has the advantage of reducing the influence of the correlation between  
548 variables when reconstructing, for instance, temperature and precipitation. This may be particularly  
549 relevant for regions with a temperature-moisture driven circulation system such as the East Asian  
550 Summer Monsoon (EASM) that can heavily affect precipitation patterns in certain regions (Herzschuh  
551 et al., 2019). Using WA-PLS\_tailored also increases the number of records that pass a significance level  
552 of  $p < 0.1$  (Telford and Birks, 2011). Providing several reconstructions based on different assumptions  
553 also allow exploring, even if only partially, the uncertainties associated with the modelling assumptions  
554 (e.g., MAT vs WA-PLS, the number of analogues, type metric used to compare pollen samples).

555 The significance tests sensu Telford and Birks (2011) revealed a rather low percentage of  
556 reconstructions to be substantial ( $p < 0.1$ ). However, a failed significance test does not necessarily mean  
557 that the reconstruction is not reliable, but the results should be treated more cautiously, as the Telford-  
558 Birks test is rather conservative (Luoto et al., 2014; Hébert et al., 2022). Several reasons of possible  
559 false negative errors are reported and discussed in the literature, including the test being supposed to  
560 be sensitive to the size of the training data, a low magnitude of an input climate signal, the trajectory of  
561 the core samples through calibration space, or poor analog situations (Luoto et al., 2014; Self et al.,  
562 2015; Andrén et al., 2015, Hébert et al., 2022).

563 All reconstruction methods used in this study heavily rely on extensive collections of modern  
564 assemblage data covering diverse climatic and environmental gradients and are applicable on a broad  
565 spatial scale. As discussed, all the methods may struggle with some intrinsic characteristics of pollen  
566 data and of pollen compilations, including complex species responses, sensitivity to spatial  
567 autocorrelation, limited analogues that may produce poor results in so-called “quantification deserts”  
568 (Chevalier, 2019), where fossil pollen is hardly preserved or nearby modern surface pollen samples are  
569 missing (Chevalier et al., 2020). However, we designed our datasets so that more methods can be  
570 included in our reconstruction scripts (<https://doi.org/10.5281/zenodo.5910989>; Herzs Schuh et al.,  
571 2022b), such as CREST, an approach that combines presence-only occurrence data from species  
572 distribution databases instead of modern pollen samples to estimate the responses of pollen taxa to the  
573 climate variable to reconstruct to a climate variable (Chevalier et al., 2014; Chevalier, 2022). CREST is,  
574 therefore, more independent from the availability of modern pollen samples. Employing the Inverse-  
575 Modelling through iterative forward modeling (IMIFM) (Izumi and Bartlein, 2016) might also be possible  
576 in such regions. Its use would be particularly interesting to reconstruct the LGM samples, because  
577 IMIFM is the only technique that can explicitly take the effect of CO<sub>2</sub> on plants (Chevalier et al., 2020).  
578 The inclusion of CREST and/or IMIFM in such large-scale studies would complement our multi-model  
579 reconstruction ensemble by exploring a larger fraction of the “method uncertainty” space in greater  
580 details (e.g. Brewer et al, 2008). Kucera et al. (2005) propose several metrics for a multi-technique  
581 approach to assess the uncertainty space: correlations between the residuals (observed minus  
582 reconstructed values) between pairs of techniques are used to investigate the similarity in the  
583 reconstructions among different techniques. The correlation between the residuals in seasonal  
584 reconstructions (e.g. summer and winter temperatures, summer and annual temperatures) can be used  
585 to investigate the degree of independence of different seasonal reconstructions. Error rate estimates

586 (RMSEP) determined by cross validation of the calibration data sets and the leaving-one-out method  
587 can be used to compare the calibration of individual transfer function techniques, though it should be  
588 considered that error estimates may vary with the choice of the cross-validation procedure (Kucera et  
589 al., 2005).

#### 591 **5.4 Potential use of LegacyClimate 1.0**

592 Our LegacyPollen 1.0 fossil pollen synthesis (Herzschuh et al., 2022c) contains records from all over  
593 the Northern Hemisphere extratropics. We used this synthesis to produce our LegacyClimate 1.0  
594 reconstruction data set. ~~Climate reconstruction data sets like LegacyClimate 1.0, which~~ thus can be  
595 used to infer spatio-temporal patterns in climate reconstructions that are not only limited to a local or  
596 regional scale. Although several hemispheric or global reconstruction studies exist, they have been  
597 largely restricted to temperature or have included relatively few records (Marcott et al., 2013; Marsicek  
598 et al., 2018; Routson et al., 2019; Kaufman et al., 2020a and 2020b). Our dataset is therefore a valuable  
599 addition. It may be used in a multi-proxy approach, synthesizing marine and terrestrial records in order  
600 to assess temperature development during the Holocene and can help to highlight possible  
601 interdependencies between oceans and land masses ~~and such contribute to the “Holocene conundrum”~~  
602 debate (Liu et al., 2014). Globally or hemispherically averaged tTemperature reconstructions from proxy  
603 data indicate peak temperatures during the Holocene Thermal Maximum around 6000 years BP followed  
604 by a pronounced cooling trend toward the late Holocene (~~Kaufman et al., 2020b~~), which is also visible  
605 in our pollen-based reconstructions (Fig. 106). Hence, spatial variability in the Holocene temperature  
606 trends (e.g. missing of a pronounced maximum for certain latitudinal bands; delayed thermal maximum  
607 on land compared to the ocean) indicate a more local rather than a global Holocene Thermal Maximum  
608 (Kaufman et al., 2020b; Osman et al., 2021; Cartapanis et al., 2022). In contrast, climate models  
609 simulate a monotonic warming throughout the Holocene, which resulted in the “Holocene conundrum”  
610 debate (Liu et al., 2014). The debate has since progressed and hints to discrepancies in data-model  
611 comparisons due to spatiotemporal dynamics related to heterogeneous responses to climate forcing  
612 and feedbacks (i.e. the timing of a Holocene Thermal Maximum in the Northern Hemisphere extra-  
613 tropics between reconstructions from continental and from marine proxy records; Cartapanis et al.,  
614 2022) and sometimes poor spatial averaging due to unevenly distributed proxies. Proxy-only  
615 reconstructions often rely on latitudinal binning and weighting, which makes this approach particularly



616 sensitive to latitudinal bands that contain only sparse spatial coverage and thus do not represent a true  
617 global average (Osman et al., 2021). Those spatiotemporal dynamics should be considered in data-  
618 model comparison.

619 Temperature reconstructions ~~are often~~ use derived from sea surface temperatures as either mean  
620 annual temperatures (Birks, 2019; Bova et al., 2021) or global mean surface temperature<sub>s</sub> (Marcott et  
621 al., 2013; Marsicek et al., 2018; Kaufman et al., 2020a and 2020b). Despite T<sub>ann</sub> being more commonly  
622 used in multi-proxy comparisons, it might be useful to also consider T<sub>July</sub>, as on a regional scale the  
623 mean July temperature (or in general summer temperature) is more important in particular in high  
624 latitudes. However, it is argued that proxy-based climate reconstructions are seasonally biased and  
625 therefore might be the reason for the observed proxy-model divergence (Liu et al., 2014; Rehfeld et al.,  
626 2016; Kaufman et al., 2020b). In this respect, it might help that we provide T<sub>July</sub> along with T<sub>ann</sub>  
627 reconstructions derived from our tailoring approach, which provides the opportunity to assess seasonal  
628 impacts on the reconstruction (especially in the high latitudes) in addition to a consistent reconstruction  
629 synthesis.

630 So far, reconstructions of precipitation have not been implemented on a hemispheric scale. The  
631 interconnection between temperature and precipitation (Trenberth, 2011) and its spatio-temporal  
632 variation across the Northern Hemisphere is therefore an important aspect of evaluating climate models  
633 (Wu et al., 2013; Hao et al., 2019; Herzsuh et al., 2022a). A broad-scale quantitative reconstruction  
634 of temperature and precipitation would therefore be of great value for evaluating transient climate model  
635 experiments such as TraCE 21k (He, 2010).

636 ~~Our assessments of the modern dataset (e.g. using CCA), the transfer function (e.g. RMSEP) and the~~  
637 ~~reconstruction (e.g. the significance test) revealed also the potential biases in the pollen-based~~  
638 ~~reconstruction and pointed to limitations. Further validation and assessments of the results and more~~  
639 ~~comprehensive uncertainty analyses e.g. by applying forward modelling approaches (Izumi & Bartlein,~~  
640 ~~2016; Parnell et al., 2016) would be highly valuable.~~

641

642

643

**644 6 Data and code availability**

645 The compilation of reconstructed  $T_{\text{July}}$ ,  $T_{\text{ann}}$ , and  $P_{\text{ann}}$ , is open access and available at PANGAEA  
646 (<https://doi.pangaea.de/10.1594/PANGAEA.930512>; in the “*Other version*” section; Herzsuh et al.,  
647 2021). The dataset files are stored in machine-readable data format (.CSV), which are already separated  
648 into Western North America, Eastern North America, Europe, and Asia for easy access and use.

649 The R code to run the reconstructions for single sites is available at Zenodo  
650 (<https://doi.org/10.5281/zenodo.5910989>; Herzsuh et al., 2022b) including harmonized open-access  
651 modern and fossil pollen datasets so that customized reconstructions can be easily established.

652

653

654

655

656

657

658

659

660

661

662

663

664

665

666

667

668

669

670

671

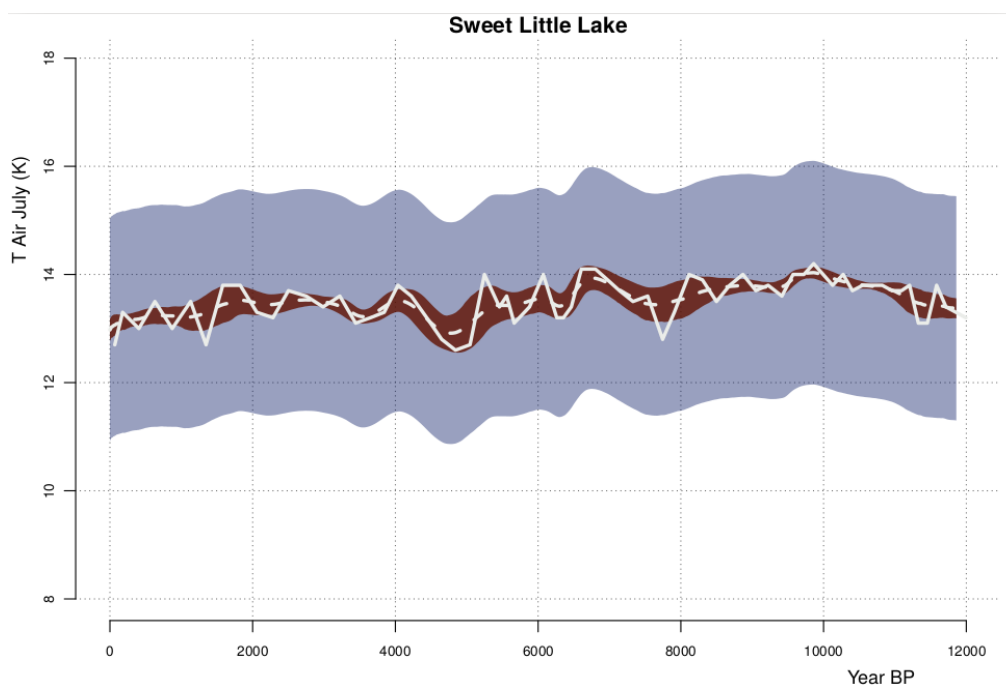
672

673

674

675

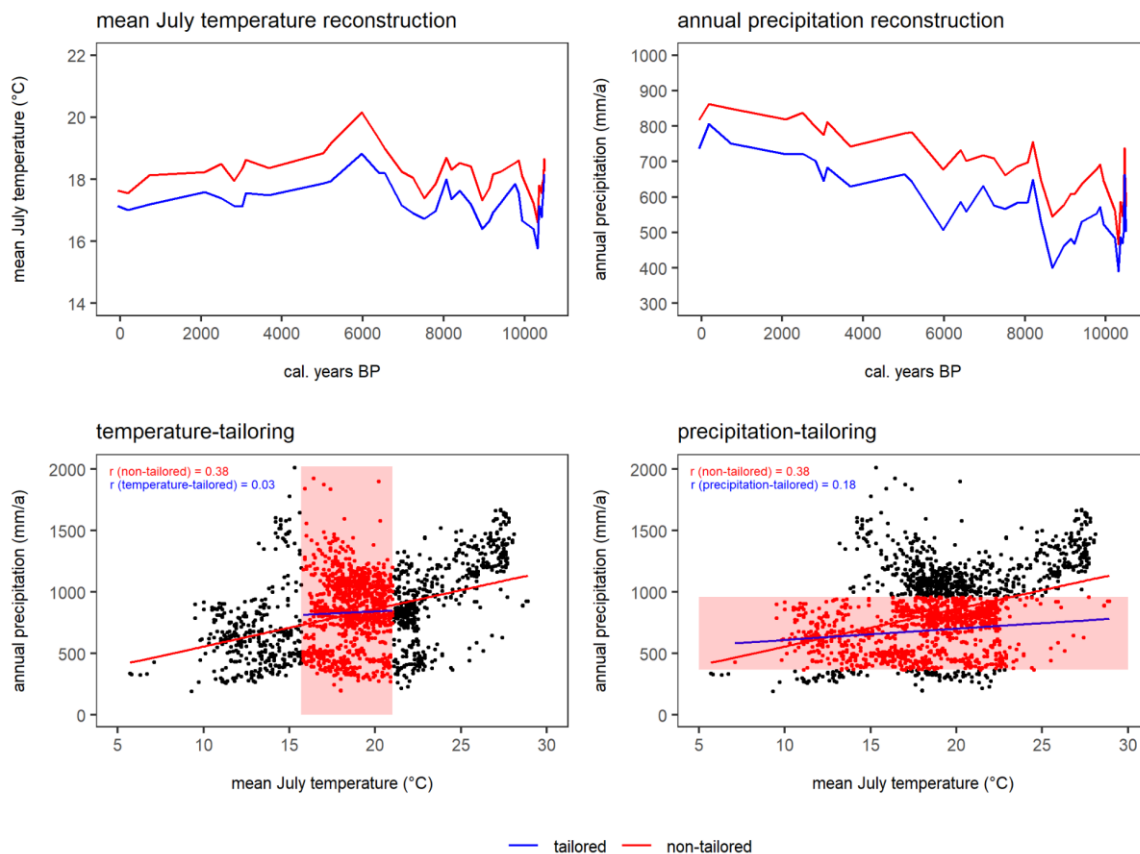
## 676 Appendix Figures



677

678 Appendix Figure 1. Reconstruction error (shaded blue) and the chronological error (shaded red) around  
679 the reconstruction smoothed by the time-uncertainty (i.e. when we interpolate at regular timesteps for  
680 the 1000 realizations and average over the ensemble, dashed white). The original reconstruction with  
681 the median ages is also shown for comparison (solid white); this underlines that averaging over the age  
682 models only preserves the low-frequencies but (unrealistically) smooths out the high-frequencies.

683



684

685 **Appendix Figure 24.** Example to illustrate the effect of tailoring the modern dataset for the location  
 686 “Yellow Dog Pond” in Eastern North America. Upper part: reconstruction of  $T_{July}$  and  $P_{ann}$  with WA-PLS  
 687 (red) and WA-PLS\_tailored (blue); lower part: correlation of  $T_{July}$  and  $P_{ann}$  in the modern dataset and the  
 688 effect of tailoring the modern dataset (indicated with the red box). Correlations are given for non-tailored  
 689 (red) and tailored (blue) data.

690

691 **Author contributions.** UH designed the study design and reconstruction dataset. CL and TB compiled  
 692 the metadata and the harmonized pollen dataset. TB wrote the R scripts and ran the analyses under the  
 693 supervision of UH. UH, TB and MC wrote the first draft of the manuscript. All authors discussed the  
 694 results and contributed to the final manuscript.

695 **Competing interests.** The contact author has declared that none of the authors has any competing  
 696 interests.

697 **Acknowledgements.** We would like to express our gratitude to all the palynologists and geologists who,  
 698 either directly or indirectly by providing their work the Neotoma Paleoeology Database, contributed

699 pollen data and chronologies to the dataset. The work of data contributors, data stewards, and the  
 700 Neotoma community is gratefully acknowledged. We thank Andrej Andreev, Mareike Wieczorek, and  
 701 Birgit Heim from AWI for providing information on pollen records and data uploads. We also thank Cathy  
 702 Jenks for language editing on a previous version of the paper.

703 **Financial support.** This research has been supported by the European Research Council (ERC Glacial  
 704 Legacy 772852 to UH) and the PalMod Initiative (01LP1510C to UH). TB and MC are supported by the  
 705 German Federal Ministry of Education and Research (BMBF) as a Research for Sustainability initiative  
 706 (FONA; <https://www.fona.de/en>) through the PalMod Phase II project (grant no. FKZ: 01LP1926D). CL  
 707 holds a scholarship from the Chinese Scholarship Council (grant no. 201908130165). NR work was  
 708 supported by the Russian Science Foundation (Grant No. 20-17-00110).

709

## 710 References

711 [Andrén, E., Klimaschewski, A., Self, A. E., St. Amour, N., Andreev, A. A., Bennett, K. D., Conley, D.](https://doi.org/10.1016/j.gloplacha.2015.02.013)  
 712 [J., Edwards, T. W. D., Solovieva, N., and Hammarlund, D.: Holocene climate and environmental](https://doi.org/10.1016/j.gloplacha.2015.02.013)  
 713 [change in north-eastern Kamchatka \(Russian Far East\), inferred from a multi-proxy study of lake](https://doi.org/10.1016/j.gloplacha.2015.02.013)  
 714 [sediments, \*Global and Planetary Change\*, 134, 41–54,](https://doi.org/10.1016/j.gloplacha.2015.02.013)  
 715 [https://doi.org/10.1016/j.gloplacha.2015.02.013, 2015.](https://doi.org/10.1016/j.gloplacha.2015.02.013)

716 Behre, K. E.: The rôle of man in European vegetation history. In: Huntley, B., Webb, T. (eds)  
 717 Vegetation history. Handbook of vegetation science, vol 7. Springer, Dordrecht.  
 718 [https://doi.org/10.1007/978-94-009-3081-0\\_17](https://doi.org/10.1007/978-94-009-3081-0_17), 1988.

719 Birks, H. J. B.: Contributions of Quaternary botany to modern ecology and biogeography, *Plant Ecol.*  
 720 *Divers.*, 12, 189–385, <https://doi.org/10.1080/17550874.2019.1646831>, 2019.

721 Birks, H. J. B., Heiri, O., Seppä, H., and Bjune, A. E.: Strengths and Weaknesses of Quantitative  
 722 Climate Reconstructions Based on Late-Quaternary, *Open Ecol. J.*, 3, 68–110,  
 723 <http://dx.doi.org/10.2174/1874213001003020068>, 2010.

724 Blaauw, M. and Christen, J. A.: Flexible paleoclimate age-depth models using an autoregressive  
 725 gamma process, *Bayesian Anal.*, 6, 457–474, <https://doi.org/10.1214/11-BA618>, 2011.

- 726 Blois, J. L., Williams, J. W., Grimm, E. C., Jackson, S. T., and Graham, R. W.: A methodological  
727 framework for assessing and reducing temporal uncertainty in paleovegetation mapping from late-  
728 Quaternary pollen records, *Quat. Sci. Rev.*, 30, 1926–1939,  
729 <https://doi.org/10.1016/j.quascirev.2011.04.017>, 2011.
- 730 Bova, S., Rosenthal, Y., Liu, Z., Godad, S. P., and Yan, M.: Seasonal origin of the thermal maxima at  
731 the Holocene and the last interglacial, *Nature*, 589, 548–553, [https://doi.org/10.1038/s41586-020-](https://doi.org/10.1038/s41586-020-03155-x)  
732 [03155-x](https://doi.org/10.1038/s41586-020-03155-x), 2021.
- 733 Brewer, S., Guiot, J., Sánchez-Goñi, M. F., and Klotz, S.: The climate in Europe during the Eemian:  
734 a multi-method approach using pollen data, *Quaternary Science Reviews*, 27, 2303–2315,  
735 <https://doi.org/10.1016/j.quascirev.2008.08.029>, 2008.
- 736 Cao, X., Ni, J., Herzschuh, U., Wang, Y., and Zhao, Y.: A late Quaternary pollen dataset from eastern  
737 continental Asia for vegetation and climate reconstructions: Set up and evaluation, *Rev. Palaeobot.*  
738 *Palynol.*, 194, 21–37, <https://doi.org/10.1016/j.revpalbo.2013.02.003>, 2013.
- 739 Cao, X., Herzschuh, U., Telford, R. J., and Ni, J.: A modern pollen–climate dataset from China and  
740 Mongolia: Assessing its potential for climate reconstruction, *Rev. Palaeobot. Palynol.*, 211, 87–96,  
741 <https://doi.org/10.1016/j.revpalbo.2014.08.007>, 2014.
- 742 Cao, X., Tian, F., Telford, R. J., Ni, J., Xu, Q., Chen, F., Liu, X., Stebich, M., Zhao, Y., Herzschuh, U.,:  
743 Impacts of the spatial extent of pollen-climate calibration-set on the absolute values, range and  
744 trends of reconstructed Holocene precipitation. *Quaternary Science Reviews* 178, 37-53.  
745 <https://doi.org/10.1016/j.quascirev.2017.10.030>, 2017.
- 746 Cao, X., Tian, F., Andreev, A., Anderson, P. M., Lozhkin, A. V., Bezrukova, E., Ni, J., Rudaya, N.,  
747 Stobbe, A., Wiczorek, M., and Herzschuh, U.: A taxonomically harmonized and temporally  
748 standardized fossil pollen dataset from Siberia covering the last 40 kyr, *Earth Syst. Sci. Data*, 12,  
749 119–135, <https://doi.org/10.5194/essd-12-119-2020>, 2020.
- 750 [Cartapanis, O., Jonkers, L., Moffa-Sanchez, P., Jaccard, S. L., and de Vernal, A.: Complex spatio-](https://doi.org/10.1038/s41467-022-33362-1)  
751 [temporal structure of the Holocene Thermal Maximum, \*Nat Commun\*, 13, 5662,](https://doi.org/10.1038/s41467-022-33362-1)  
752 <https://doi.org/10.1038/s41467-022-33362-1>, 2022.

- 753 Chen, F., Chen, J., Huang, W., Chen, S., Huang, X., Jin, L., Jia, J., Zhang, X., An, C., Zhang, J., Zhao,  
754 Y., Yu, Z., Zhang, R., Liu, J., Zhou, A., and Feng, S.: Westerlies Asia and monsoonal Asia:  
755 Spatiotemporal differences in climate change and possible mechanisms on decadal to sub-orbital  
756 timescales, *Earth Sci. Rev.*, 192, 337–354, <https://doi.org/10.1016/j.earscirev.2019.03.005>, 2019.
- 757 Chevalier, M.: Enabling possibilities to quantify past climate from fossil assemblages at a global scale,  
758 *Glob. Planet. Change*, 175, 27–35, <https://doi.org/10.1016/j.gloplacha.2019.01.016>, 2019.
- 759 Chevalier, M.: *crestr*: an R package to perform probabilistic climate reconstructions from  
760 palaeoecological datasets, *Clim. Past*, 18, 821–844, <https://doi.org/10.5194/cp-18-821-2022>, 2022.
- 761 Chevalier, M., Cheddadi, R., and Chase, B. M.: CREST (Climate REconstruction SofTware): a  
762 probability density function (PDF)-based quantitative climate reconstruction method, *Clim. Past*, 10,  
763 2081–2098, <https://doi.org/10.5194/cp-10-2081-2014>, 2014.
- 764 Chevalier, M., Davis, B. A. S., Heiri, O., Seppä, H., Chase, B. M., Gajewski, K., Lacourse, T., Telford,  
765 R. J., Finsinger, W., Guiot, J., Köhl, N., Maezumi, S. Y., Tipton, J. R., Carter, V. A., Brussel, T.,  
766 Phelps, L. N., Dawson, A., Zanon, M., Vallé, F., Nolan, C., Mauri, A., de Vernal, A., Izumi, K.,  
767 Holmström, L., Marsicek, J., Goring, S., Sommer, P. S., Chaput, M., and Kupriyanov, D.: Pollen-  
768 based climate reconstruction techniques for late Quaternary studies, *Earth Sci. Rev.*, 210, 103384,  
769 <https://doi.org/10.1016/j.earscirev.2020.103384>, 2020.
- 770 Davis, B. A. S., Zanon, M., Collins, P., Mauri, A., Bakker, J., Barboni, D., Barthelmes, A., Beaudouin,  
771 C., Bjune, A. E., Bozilova, E., Bradshaw, R. H. W., Brayshay, B. A., Brewer, S., Brugiapaglia, E.,  
772 Bunting, J., Connor, S. E., de Beaulieu, J.-L., Edwards, K., Ejarque, A., Fall, P., Florenzano, A.,  
773 Fyfe, R., Galop, D., Giardini, M., Giesecke, T., Grant, M. J., Guiot, J., Jahns, S., Jankovská, V.,  
774 Juggins, S., Kahrman, M., Karpińska-Kołaczek, M., Kołaczek, P., Köhl, N., Kuneš, P., Lapteva, E.  
775 G., Leroy, S. A. G., Leydet, M., Guiot, J., Jahns, S., Jankovská, V., Juggins, S., Kahrman, M.,  
776 Karpińska-Kołaczek, M., Kołaczek, P., Köhl, N., Kuneš, P., Lapteva, E. G., Leroy, S. A. G., Leydet,  
777 M., López Sáez, J. A., Masi, A., Matthias, I., Mazier, F., Meltsov, V., Mercuri, A. M., Miras, Y.,  
778 Mitchell, F. J. G., Morris, J. L., Naughton, F., Nielsen, A. B., Novenko, E., Odgaard, B., Ortu, E.,  
779 Overballe-Petersen, M. V., Pardoe, H. S., Peglar, S. M., Pidek, I. A., Sadori, L., Seppä, H.,  
780 Severova, E., Shaw, H., Święta-Musznicka, J., Theuerkauf, M., Tonkov, S., Veski, S., van der

- 781 Knaap, W. O., van Leeuwen, J. F. N., Woodbridge, J., Zimny, M., and Kaplan, J. O.: The European  
782 Modern Pollen Database (EMPD) project, *Veg. Hist. Archaeobot.*, 22, 521–530,  
783 <https://doi.org/10.1007/s00334-012-0388-5>, 2013.
- 784 Davis, B. A. S., Chevalier, M., Sommer, P., Carter, V. A., Finsinger, W., Mauri, A., Phelps, L. N.,  
785 Zanon, M., Abegglen, R., Åkesson, C. M., Alba-Sánchez, F., Anderson, R. S., Antipina, T. G.,  
786 Atanassova, J. R., Beer, R., Belyanina, N. I., Blyakharchuk, T. A., Borisova, O. K., Bozilova, E.,  
787 Bukreeva, G., Bunting, M. J., Clò, E., Colombaroli, D., Combourieu-Nebout, N., Desprat, S., Di Rita,  
788 F., Djamali, M., Edwards, K. J., Fall, P. L., Feurdean, A., Fletcher, W., Florenzano, A., Furlanetto,  
789 G., Gaceur, E., Galimov, A. T., Gałka, M., García-Moreiras, I., Giesecke, T., Grindean, R., Guido,  
790 M. A., Gvozdeva, I. G., Herzschuh, U., Hjelle, K. L., Ivanov, S., Jahns, S., Jankovska, V., Jiménez-  
791 Moreno, G., Karpińska-Kołaczek, M., Kitaba, I., Kołaczek, P., Lapteva, E. G., Latałowa, M.,  
792 Lebreton, V., Leroy, S., Leydet, M., Lopatina, D. A., López-Sáez, J. A., Lotter, A. F., Magri, D.,  
793 Marinova, E., Matthias, I., Mavridou, A., Mercuri, A. M., Mesa-Fernández, J. M., Mikishin, Y. A.,  
794 Milecka, K., Montanari, C., Morales-Molino, C., Mrotzek, A., Muñoz Sobrino, C., Naidina, O. D.,  
795 Nakagawa, T., Nielsen, A. B., Novenko, E. Y., Panajiotidis, S., Panova, N. K., Papadopoulou, M.,  
796 Pardoe, H. S., Pędziszewska, A., Petrenko, T. I., Ramos-Román, M. J., Ravazzi, C., Rösch, M.,  
797 Ryabogina, N., Sabariego Ruiz, S., Salonen, J. S., Sapelko, T. V., Schofield, J. E., Seppä, H.,  
798 Shumilovskikh, L., Stivrins, N., Stojakowits, P., Svobodova Svitavska, H., Święta-Musznicka, J.,  
799 Tantau, I., Tinner, W., Tobolski, K., Tonkov, S., Tsakiridou, M., et al.: The Eurasian Modern Pollen  
800 Database (EMPD), version 2, *Earth Syst. Sci. Data*, 12, 2423–2445, [https://doi.org/10.5194/essd-](https://doi.org/10.5194/essd-12-2423-2020)  
801 [12-2423-2020](https://doi.org/10.5194/essd-12-2423-2020), 2020.
- 802 Eyring, V., Cox, P. M., Flato, G. M., Gleckler, P. J., Abramowitz, G., Caldwell, P., Collins, W. D., Gier,  
803 B. K., Hall, A. D., Hoffman, F. M., Hurtt, G. C., Jahn, A., Jones, C. D., Klein, S. A., Krasting, J. P.,  
804 Kwiatkowski, L., Lorenz, R., Maloney, E., Meehl, G. A., Pendergrass, A. G., Pincus, R., Ruane, A.  
805 C., Russell, J. L., Sanderson, B. M., Santer, B. D., Sherwood, S. C., Simpson, I. R., Stouffer, R. J.,  
806 and Williamson, M. S.: Taking climate model evaluation to the next level, *Nat. Clim. Chang.*, 9, 102–  
807 110, <https://doi.org/10.1038/s41558-018-0355-y>, 2019.
- 808 Fick, S. E. and Hijmans, R. J.: WorldClim 2: new 1-km spatial resolution climate surfaces for global  
809 land areas, *Int. J. Climatol.*, 37, 4302–4315, <https://doi.org/10.1002/joc.5086>, 2017.



- 810 Gajewski, K., Vance, R., Sawada, M., Fung, I., Gignac, L. D., Halsey, L., John, J., Maisongrande, P.,  
811 Mandell, P., Mudie, P. J., Richard, P. J. H., Sherin, A. G., Soroko, J., and Vitt, D. H.: The climate of  
812 North America and adjacent ocean waters ca. 6 ka. *Canadian Journal of Earth Sciences* 37.5: 661-  
813 681, 2000.
- 814 Hao, Z., Phillips, T. J., Hao, F., and Wu, X.: Changes in the dependence between global precipitation  
815 and temperature from observations and model simulations, *Int. J. Climatol.*, 39, 4895–4906,  
816 <https://doi.org/10.1002/joc.6111>, 2019.
- 817 He, F.: Simulating transient climate evolution of the last deglaciation with CCSM3, Ph.D. thesis,  
818 University of Wisconsin-Madison, USA, 185 pp., 2010.
- 819 [Hébert, R., Herzschuh, U., and Laepple, T.: Millennial-scale climate variability over land overprinted](#)  
820 [by ocean temperature fluctuations, \*Nat. Geosci.\*, 15, 899–905, \[https://doi.org/10.1038/s41561-022-\]\(https://doi.org/10.1038/s41561-022-01056-4\)](#)  
821 [01056-4, 2022.](#)
- 822 Herzschuh, U., Cao, X., Laepple, T., Dallmeyer, A., Telford, R. J., Ni, J., Chen, F., Kong, Z., Liu, G.,  
823 Liu, K.-B., Liu, X., Stebich, M., Tang, L., Tian, F., Wang, Y., Wischnewski, J., Xu, Q., Yan, S., Yang,  
824 Z., Yu, G., Zhang, Y., Zhao, Y., and Zheng, Z.: Position and orientation of the westerly jet  
825 determined Holocene rainfall patterns in China, *Nat. Commun.*, 10, 2376,  
826 <https://doi.org/10.1038/s41467-019-09866-8>, 2019.
- 827 Herzschuh, U., Böhmer, T., Li, C., and Cao, X.: Northern Hemisphere temperature and precipitation  
828 reconstruction from taxonomically harmonized pollen data set with revised chronologies using WA-  
829 PLS and MAT (LegacyClimate 1.0), PANGAEA,  
830 <https://doi.pangaea.de/10.1594/PANGAEA.930512>, 2021.
- 831 Herzschuh, U., Böhmer, T., Li, C., Cao, X., Hébert, R., Dallmeyer, A., Telford, R. J., Kruse, S.:  
832 Reversals in temperature-precipitation correlations in the Northern Hemisphere extratropics during  
833 the Holocene. *Geophysical Research Letters*, p.e2022GL099730,  
834 <https://doi.org/10.1029/2022GL099730>, 2022a.
- 835 Herzschuh, U., Böhmer, T., Li, C., Chevalier, M., Dallmeyer, A., Cao, X., Bigelow, N. H., Nazarova,  
836 L., Novenko, E. Y., Park, J., Peyron, O., Rudaya, N. A., Schlütz, F., Shumilovskikh, L. S., Tarasov,

- 837 P. E., Wang, Y., Wen, R., Xu, Q., and Zheng, Z.: LegacyClimate 1.0: A dataset of pollen-based  
838 climate reconstructions from 2594 Northern Hemisphere sites covering the late Quaternary [Data  
839 set], Zenodo, <https://doi.org/10.5281/zenodo.5910989>, 2022b.
- 840 Herzs Schuh, U., Li, C., Böhmer, T., Postl, A. K., Heim, B., Andreev, A. A., Cao, X., Wiczorek, M., and  
841 Ni, J.: LegacyPollen 1.0: a taxonomically harmonized global late Quaternary pollen dataset of 2831  
842 records with standardized chronologies, *Earth Syst. Sci. Data*, 14, 3213–3227,  
843 <https://doi.org/10.5194/essd-14-3213-2022>, 2022c.
- 844 Hijmans, R. J., van Etten, J., Sumner, M., Cheng, J., Baston, D., Bevan, A., Bivand, R., Busetto, L.,  
845 Canty, M., Fasoli, B., Forrest, D., Ghosh, A., Golicher, D., Gray, J., Greenberg, J. A., Hiemstra, P.,  
846 Hingee, K., Ilich, A., Institute for Mathematics Applied Geosciences, Karney, C., Mattiuzzi, M.,  
847 Mosher, S., Naimi, B., Nowosad, J., Pebesma, E., Lamigueiro, O. P., Racine, E. B., Rowlingson,  
848 B., Shortridge, A., Venables, B., and Wueest, R.: Raster: Geographic Data Analysis and Modeling,  
849 R package version 3.5-11, <https://cran.r-project.org/web/packages/raster>, 2021.
- 850 Hill, M. O.: Diversity and Evenness: A Unifying Notation and Its Consequences, *Ecology*, 54, 427–  
851 432, <https://doi.org/10.2307/1934352>, 1973.
- 852 Izumi, K. and Bartlein, P. J.: North American paleoclimate reconstructions for the Last Glacial  
853 Maximum using an inverse modeling through iterative forward modeling approach applied to pollen  
854 data: Pollen-Based Climate Reconstruction, *Geophys. Res. Lett.*, 43, 10,965-10,972,  
855 <https://doi.org/10.1002/2016GL070152>, 2016.
- 856 Jackson, S. T.: Pollen source area and representation in small lakes of the northeastern United States,  
857 *Rev. Palaeobot. Palynol.*, 63, 53–76, [https://doi.org/10.1016/0034-6667\(90\)90006-5](https://doi.org/10.1016/0034-6667(90)90006-5), 1990.
- 858 Jackson, S. T. and Williams, J. W.: MODERN ANALOGS IN QUATERNARY PALEOECOLOGY: Here  
859 Today, Gone Yesterday, Gone Tomorrow?, *Annu. Rev. Earth Planet. Sci.*, 32, 495–537,  
860 <https://doi.org/10.1146/annurev.earth.32.101802.120435>, 2004.
- 861 Juggins, S.: Quantitative reconstructions in palaeolimnology: new paradigm or sick science?,  
862 *Quaternary Science Reviews*, 64, 20–32, <https://doi.org/10.1016/j.quascirev.2012.12.014>, 2013.

- 863 Juggins, S.: rioja: Analysis of Quaternary Science Data, R package version 0.9-21, [https://cran.r-](https://cran.r-project.org/web/packages/rioja)  
864 [project.org/web/packages/rioja](https://cran.r-project.org/web/packages/rioja), 2019.
- 865 Kaufman, D., McKay, N., Routson, C., Erb, M., Davis, B., Heiri, O., Jaccard, S., Tierney, J., Dätwyler,  
866 C., Axford, Y., Brussel, T., Cartapanis, O., Chase, B., Dawson, A., de Vernal, A., Engels, S.,  
867 Jonkers, L., Marsicek, J., Moffa-Sánchez, P., Morrill, C., Orsi, A., Rehfeld, K., Saunders, K.,  
868 Sommer, P. S., Thomas, E., Tonello, M., Tóth, M., Vachula, R., Andreev, A., Bertrand, S.,  
869 Biskaborn, B., Bringué, M., Brooks, S., Caniupán, M., Chevalier, M., Cwynar, L., Emile-Geay, J.,  
870 Fegyveresi, J., Feurdean, A., Finsinger, W., Fortin, M.-C., Foster, L., Fox, M., Gajewski, K.,  
871 Grosjean, M., Hausmann, S., Heinrichs, M., Holmes, N., Ilyashuk, B., Ilyashuk, E., Juggins, S.,  
872 Khider, D., Koinig, K., Langdon, P., Larocque-Tobler, I., Li, J., Lotter, A., Luoto, T., Mackay, A.,  
873 Magyari, E., Malevich, S., Mark, B., Massaferró, J., Montade, V., Nazarova, L., Novenko, E., Pařil,  
874 P., Pearson, E., Peros, M., Pienitz, R., Płóciennik, M., Porinchu, D., Potito, A., Rees, A.,  
875 Reinemann, S., Roberts, S., Rolland, N., Salonen, S., Self, A., Seppä, H., Shala, S., St-Jacques,  
876 J.-M., Stenni, B., Syrykh, L., Tarrats, P., Taylor, K., van den Bos, V., Velle, G., Wahl, E., Walker, I.,  
877 Wilmshurst, J., Zhang, E., and Zhilich, S.: A global database of Holocene paleotemperature records,  
878 *Sci. Data*, 7, 115, <https://doi.org/10.1038/s41597-020-0445-3>, 2020a.
- 879 Kaufman, D., McKay, N., Routson, C., Erb, M., Dätwyler, C., Sommer, P. S., Heiri, O., and Davis, B.:  
880 Holocene global mean surface temperature, a multi-method reconstruction approach, *Sci. Data*, 7,  
881 201, <https://doi.org/10.1038/s41597-020-0445-3>, 2020b.
- 882 [Kucera, M., Weinelt, M., Kiefer, T., Pflaumann, U., Hayes, A., Weinelt, M., Chen, M.-T., Mix, A. C.,](#)  
883 [Barrows, T. T., Cortijo, E., Duprat, J., Juggins, S., and Waelbroeck, C.: Reconstruction of sea-](#)  
884 [surface temperatures from assemblages of planktonic foraminifera: multi-technique approach](#)  
885 [based on geographically constrained calibration data sets and its application to glacial Atlantic and](#)  
886 [Pacific Oceans, \*Quaternary Science Reviews\*, 24, 951–998,](#)  
887 [<https://doi.org/10.1016/j.quascirev.2004.07.014>, 2005.](#)
- 888 Li, C., Postl, A. K., Böhmer, T., Cao, X., Dolman, A. M., and Herzschuh, U.: Harmonized chronologies  
889 of a global late Quaternary pollen dataset (LegacyAge 1.0), *Earth Syst. Sci. Data*, 14, 1331–1343,  
890 <https://doi.org/10.5194/essd-14-1331-2022>, 2022.

891 Liu, Z., Zhu, J., Rosenthal, Y., Zhang, X., Otto-Bliesner, B. L., Timmermann, A., Smith, R. S.,  
892 Lohmann, G., Zheng, W., and Timm, O. E.: The Holocene temperature conundrum, PNAS, 111,  
893 E3501–E3505, <https://doi.org/10.1073/pnas.1407229111>, 2014.

894 [Luoto, T. P., Kaukolehto, M., Weckström, J., Korhola, A., and Väliranta, M.: New evidence of warm](#)  
895 [early-Holocene summers in subarctic Finland based on an enhanced regional chironomid-based](#)  
896 [temperature calibration model, Quat. res., 81, 50–62, <https://doi.org/10.1016/j.yqres.2013.09.010>,](#)  
897 [2014.](#)

898 Marcott, S. A., Shakun, J. D., Clark, P. U., and Mix, A. C.: A Reconstruction of Regional and Global  
899 Temperature for the Past 11,300 Years, Science, 339, 1198–1201,  
900 <https://doi.org/10.1126/science.1228026>, 2013.

901 Marsicek, J., Shuman, B. N., Bartlein, P. J., Shafer, S. L., and Brewer, S.: Reconciling divergent trends  
902 and millennial variations in Holocene temperatures, Nature, 554, 92–96,  
903 <https://doi.org/10.1038/nature25464>, 2018.

904 Mauri, A., Davis, B. A. S., Collins, P. M., and Kaplan, J. O.: The climate of Europe during the Holocene:  
905 a gridded pollen-based reconstruction and its multi-proxy evaluation, Quat. Sci. Rev., 112, 109–  
906 127, <https://doi.org/10.1016/j.quascirev.2015.01.013>, 2015.

907 Nychka, D., Furrer, R., Paige, J., Sain, S., Gerber, F., and Iverson, M.: fields: Tools for Spatial Data,  
908 R package version 10.3, <https://cran.r-project.org/web/packages/fields/index.html>, 2020.

909 Oksanen, J., Blanchet, F. G., Friendly, M., Kindt, R., Legendre, P., McGlinn, D., Minchin, P. R.,  
910 O'Hara, R. B., Simpson, G. L., Solymos, P., Stevens, M. H. H., Szoecs, E., and Wagner, H.: Vegan:  
911 Community Ecology Package, R package version 2.5-7, [https://cran.r-](https://cran.r-project.org/web/packages/vegan)  
912 [project.org/web/packages/vegan](https://cran.r-project.org/web/packages/vegan), 2020.

913 [Osman, M. B., Tierney, J. E., Zhu, J., Tardif, R., Hakim, G. J., King, J., and Poulsen, C. J.: Globally](#)  
914 [resolved surface temperatures since the Last Glacial Maximum, Nature, 599, 239–244,](#)  
915 <https://doi.org/10.1038/s41586-021-03984-4>, 2021.

- 916 Overpeck, J. T., Webb, T., and Prentice, I. C.: Quantitative Interpretation of Fossil Pollen Spectra:  
917 Dissimilarity Coefficients and the Method of Modern Analogs, *Quat. Res.*, 23, 87–108,  
918 [https://doi.org/10.1016/0033-5894\(85\)90074-2](https://doi.org/10.1016/0033-5894(85)90074-2), 1985.
- 919 Parnell, A. C., Haslett, J., Sweeney, J., Doan, T. K., Allen, J. R. M., and Huntley, B.: Joint  
920 palaeoclimate reconstruction from pollen data via forward models and climate histories, *Quaternary*  
921 *Science Reviews*, 151, 111–126, <https://doi.org/10.1016/j.quascirev.2016.09.007>, 2016.
- 922 R Core Team: R: A language and environment for statistical computing, R Foundation for Statistical  
923 Computing, Vienna, Austria, available online at: <https://www.R-project.org/>, 2020.
- 924 Rehfeld, K., Trachsel, M., Telford, R. J., and Laepple, T.: Assessing performance and seasonal bias  
925 of pollen-based climate reconstructions in a perfect model world, *Clim. Past*, 12, 2255–2270,  
926 <https://doi.org/10.5194/cp-12-2255-2016>, 2016.
- 927 Routson, C. C., McKay, N. P., Kaufman, D. S., Erb, M. P., Goosse, H., Shuman, B. N., Rodysill, J. R.,  
928 and Ault, T.: Mid-latitude net precipitation decreased with Arctic warming during the Holocene,  
929 *Nature*, 568, 83–87, <https://doi.org/10.1038/s41586-019-1060-3>, 2019.
- 930 [Self, A. E., Jones, V. J., and Brooks, S. J.: Late Holocene environmental change in arctic western](#)  
931 [Siberia, \*The Holocene\*, 25, 150–165, <https://doi.org/10.1177/0959683614556387>, 2015.](#)
- 932 Simpson, G. L.: Analogue Methods in Palaeolimnology, in: *Tracking Environmental Change Using*  
933 *Lake Sediments: Data Handling and Numerical Techniques*, edited by: Birks, H. J. B., Lotter, A. F.,  
934 Juggins, S., and Smol, J. P., Springer Netherlands, Dordrecht, 495–522,  
935 [https://doi.org/10.1007/978-94-007-2745-8\\_15](https://doi.org/10.1007/978-94-007-2745-8_15), 2012.
- 936 Simpson, G. L., Oksanen, J., Maechler, M.: analogue: Analogue and Weighted Averaging Methods  
937 for Palaeoecology, R package version 0.17-6, <https://cran.r-project.org/web/packages/analogue/>,  
938 2021.
- 939 Sugita, S.: A Model of Pollen Source Area for an Entire Lake Surface, *Quat. Res.*, 39, 239–244,  
940 <https://doi.org/10.1006/qres.1993.1027>, 1993.

- 941 Tarasov, P. E., Nakagawa, T., Demske, D., Österle, H., Igarashi, Y., Kitagawa, J., Mokhova, L.,  
942 Bazarova, V., Okuda, M., Gotanda, K., Miyoshi, N., Fujiki, T., Takemura, K., Yonenobu, H., and  
943 Fleck, A.: Progress in the reconstruction of Quaternary climate dynamics in the Northwest Pacific:  
944 A new modern analogue reference dataset and its application to the 430-kyr pollen record from  
945 Lake Biwa, *Earth Sci. Rev.*, 108, 64–79, <https://doi.org/10.1016/j.earscirev.2011.06.002>, 2011.
- 946 Telford, R. J.: palaeoSig: Significance Tests for Palaeoenvironmental Reconstructions, R package  
947 version 2.0-3, <https://cran.r-project.org/web/packages/palaeoSig>, 2019.
- 948 Telford, R. J. and Birks, H. J. B.: A novel method for assessing the statistical significance of  
949 quantitative reconstructions inferred from biotic assemblages, *Quat. Sci. Rev.*, 30, 1272–1278,  
950 <https://doi.org/10.1016/j.quascirev.2011.03.002>, 2011.
- 951 ter Braak, C. J. F.: CANOCO - a FORTRAN program for canonical community ordination by (Partial)  
952 (Detrended) (Canonical) correspondence analysis and redundancy analysis. Agricultural  
953 Mathematics Group, Wageningen, 1988.
- 954 ter Braak, C. J. F. and Juggins, S.: Weighted averaging partial least squares regression (WA-PLS):  
955 an improved method for reconstructing environmental variables from species assemblages,  
956 *Hydrobiologia*, 269, 485–502, <https://doi.org/10.1007/BF00028046>, 1993.
- 957 Tian, F., Cao, X., Dallmeyer, A., Zhao, Y., Ni, J., and Herzschuh, U.: Pollen-climate relationships in  
958 time (9 ka, 6 ka, 0 ka) and space (upland vs. lowland) in eastern continental Asia, *Quat. Sci. Rev.*,  
959 156, 1–11, <https://doi.org/10.1016/j.quascirev.2016.11.027>, 2017.
- 960 Trachsel, M. and Telford, R. J.: All age–depth models are wrong, but are getting better, *Holocene*, 27,  
961 860–869, <https://doi.org/10.1177/0959683616675939>, 2017.
- 962 Trenberth, K. E.: Changes in precipitation with climate change, *Clim. Res.*, 47, 123–138,  
963 <https://doi.org/10.3354/cr00953>, 2011.
- 964 Whitmore, J., Gajewski, K., Sawada, M., Williams, J. W., Shuman, B., Bartlein, P. J., Minckley, T.,  
965 Viau, A. E., Webb, T., Shafer, S., Anderson, P., and Brubaker, L.: Modern pollen data from North  
966 America and Greenland for multi-scale paleoenvironmental applications, *Quat. Sci. Rev.*, 24, 1828–  
967 1848, <https://doi.org/10.1016/j.quascirev.2005.03.005>, 2005.

968 Williams, J. W., Grimm, E. C., Blois, J. L., Charles, D. F., Davis, E. B., Goring, S. J., Graham, R. W.,  
969 Smith, A. J., Anderson, M., Arroyo-Cabrales, J., Ashworth, A. C., Betancourt, J. L., Bills, B. W.,  
970 Booth, R. K., Buckland, P. I., Curry, B. B., Giesecke, T., Jackson, S. T., Latorre, C., Nichols, J.,  
971 Purdum, T., Roth, R. E., Stryker, M., and Takahara, H.: The Neotoma Paleoecology Database, a  
972 multiproxy, international, community-curated data resource, *Quat. Res.*, 89, 156–177,  
973 <https://doi.org/10.1017/qua.2017.105>, 2018.

974 Williams, J. W., Webb III, T., Richard, P. H., and Newby, P.: Late Quaternary biomes of Canada and  
975 the eastern United States, *J. Biogeogr.*, 27, 585–607, [https://doi.org/10.1046/j.1365-](https://doi.org/10.1046/j.1365-2699.2000.00428.x)  
976 [2699.2000.00428.x](https://doi.org/10.1046/j.1365-2699.2000.00428.x), 2000.

977 Wu, R., Chen, J., and Wen, Z.: Precipitation-surface temperature relationship in the IPCC CMIP5  
978 models, *Adv. Atmos. Sci.*, 30, 766–778, <https://doi.org/10.1007/s00376-012-2130-8>, 2013.

979 [Zanon, M., Davis, B. A. S., Marquer, L., Brewer, S., and Kaplan, J. O.: European Forest Cover During](#)  
980 [the Past 12,000 Years: A Palynological Reconstruction Based on Modern Analogs and Remote](#)  
981 [Sensing, \*Front. Plant Sci.\*, 9, 253, <https://doi.org/10.3389/fpls.2018.00253>, 2018.](#)